



Analysis of the equilibrium phase in immune-controlled tumors predicts best strategies for cancer treatment

Kevin Atsou, Sokchea Khou, Fabienne Anjuère, Veronique Braud, Thierry Goudon

► To cite this version:

Kevin Atsou, Sokchea Khou, Fabienne Anjuère, Veronique Braud, Thierry Goudon. Analysis of the equilibrium phase in immune-controlled tumors predicts best strategies for cancer treatment. 2021. hal-03115518

HAL Id: hal-03115518

<https://hal.science/hal-03115518>

Preprint submitted on 19 Jan 2021

HAL is a multi-disciplinary open access archive for the deposit and dissemination of scientific research documents, whether they are published or not. The documents may come from teaching and research institutions in France or abroad, or from public or private research centers.

L'archive ouverte pluridisciplinaire **HAL**, est destinée au dépôt et à la diffusion de documents scientifiques de niveau recherche, publiés ou non, émanant des établissements d'enseignement et de recherche français ou étrangers, des laboratoires publics ou privés.

Analysis of the equilibrium phase in immune-controlled tumors predicts best strategies for cancer treatment

Kevin Atsou ¹, Sokchea Khou ^{2,3}, Fabienne Anjuère ², Véronique M. Braud ^{2*†}
and Thierry Goudon ^{1*†}

¹*Univ. Côte d'Azur, Inria, CNRS, LJAD, Parc Valrose, Nice, France*

²*Université Côte d'Azur, CNRS Institut de Pharmacologie Moléculaire et Cellulaire UMR 7275
660 Route des Lucioles, F-06560 Valbonne, France*

³*Department of Cell, Developmental & Cancer Biology Oregon Health & Science University
3181 SW Sam Jackson Park Road, Portland, OR, 97239, USA*

Abstract

Extensive research and clinical trials have improved our understanding of tumor immunology but despite considerable clinical benefits, current immunotherapies only provide durable responses in a minority of patients. The challenge is to identify key biological parameters preventing immune escape and maintaining an equilibrium state characterized by a stable subclinical tumor mass. Based on a space and size structured partial differential equation model, we developed numerical methods to predict the parameters of the equilibrium without running simulations of the evolution problem. By using global sensitivity analysis methods, we identified the elimination rate of tumor cells by immune cells as the leading parameter influencing the equilibrium size of the tumor and combined therapies that sustain and strengthen the anti-tumor immune response as most effective. Applied to the biological parameters that define a cancer type, such numerical investigation can provide hints for the design and optimization of cancer treatments.

Significance: Based on a space and size structured PDE model, the analyses of the equilibrium phase in immune surveillance of cancer provide numerical methods to evaluate the influence of immune response and tumor growth parameters and hints for the design and optimization of cancer treatments.

Keywords: cancer, equilibrium phase, immunotherapy, mathematical model, drug response

Introduction

The immune system plays a major role in the control of tumor growth. This has led to the concept of immune surveillance and cancer immunoediting composed of three phases [1]: the elimination, when tumors are rapidly eradicated by the immune system, the equilibrium, a latency period when tumors can survive but remain on a controlled state, and the escape, the final outgrowth of tumors that have outstripped immunological restraints. In this later phase, immune suppression is prevailing and immune cells are also subverted to promote tumor growth. Numerous cancer immunotherapy strategies have been designed and assessed to counteract cancer immune evasion and restore effective and durable elimination of tumors [2–6]. They show improved efficacy over

conventional anticancer treatments but only a minority of patients respond. The challenge to face now is to identify key biological parameters which will convert a fatal outcome into a chronic, manageable state, the durable maintenance of cancer in a viable equilibrium phase controlled by immunity. Reaching an equilibrium stage in immune-controlled tumors is indeed the first key step for successful control of tumor growth and a goal for immunotherapy. It is however difficult to apprehend experimentally because the tumor mass at equilibrium is below detectable limits [7]. Mathematical modeling of the tumor-immune system interactions offers useful information about the features of the equilibrium phase during primary tumor development, and can guide the design of optimal anticancer therapies [8–11].

We previously [8] introduced a specific mathematical model based on partial differential equations, intended to describe the earliest stages of tumor-immune system interactions. The originality of the model is to introduce size-space structured quantities, providing new perspectives compared to mere ordinary differential systems [9, 12–14]. The model thus accounts for both the growth of the tumor, by natural cell

*Corresponding author. E-mail: braud@ipmc.cnrs.fr, thierry.goudon@inria.fr

†V. M. Braud and T. Goudon contributed equally to this article.

growth and cell divisions, and the displacement of the immune cells towards the tumor, by means of activation processes and chemotaxis effects. The most notable finding is that an equilibrium state, with residual tumor and active immune cells, can be observed. Thus, mathematical analysis provides a basis for the explanation of the formation of the equilibrium. Indeed, the equilibrium can be mathematically interpreted by means of an eigenproblem coupled to a stationary diffusion equation with constraint. This observation permits us to develop an efficient numerical strategy to determine *a priori* the shape of the equilibrium — namely, the size distribution of the tumor cells and the residual tumor mass — for a given set of biological tumor and immune cell parameters. Consequently, the equilibrium state can be computed at low numerical cost since we can avoid the resolution of the evolution problem on a long time range. The use of this simple and fast algorithm allows us to address the question of the sensitivity of the residual mass to the parameters and to discuss the impact of treatments. This information can be decisive to design clinical studies and choose therapeutic strategies. Our work therefore provides a tool for cancer treatment management.

Quick guide to equations: A coupled PDE model for tumor-immune system interactions

The principles of the modeling adopted in [8] led to couple an evolution equation for the size-distribution of the tumor cells, and a convection-diffusion equation for the activated immune cells. The two-way coupling arose by the death term induced by the action of the immune cells on the tumor cells, and by the activation and the attraction of immune cells towards the tumor, which are determined by the total mass of the tumor. The unknowns are

- the size density of tumor cells $(t, z) \mapsto n(t, z)$ so that the integral $\int_a^b zn(t, z) dz$ gives the volume of the tumor occupied at time t by cells having their size z in the interval (a, b) ;
- the concentration of activated immune cells which are fighting against the tumor $(t, x) \mapsto c(t, x)$;
- the concentration of chemical signal that attracts the immune cells towards the tumor microenvironment $(t, x) \mapsto \phi(t, x)$.

The model assumes that the tumor is located at the center of a domain Ω , and it distinguishes two distinct length scales. The size of the tumor cells $z \geq 0$ is considered as “infinitely small” compared to the scale of displacement of the immune cells, described by the space variable $x \in \Omega$. Immune cells, once activated, are subjected to natural diffusion and to a chemotactic drift, induced by the presence of the tumor. The strength of this drift, as well as the activation of immune cells, directly depends on the total mass of the tumor, proportional

to the quantity

$$\mu_1(t) = \int_0^\infty zn(t, z) dz.$$

The immune system-tumor competition is described by the following system of PDEs

$$\partial_t n + \partial_z(Vn) = Q(n) - m(n, c), \quad (1a)$$

$$\partial_t c + \nabla_x \cdot (c\chi \nabla_x \phi - D\nabla_x c) = \mu_1 R - \gamma c, \quad (1b)$$

$$-\mathcal{K}\Delta_x \phi = \mu_1 \left(\sigma(x) - \frac{1}{|\Omega|} \int_\Omega \sigma(y) dy \right), \quad (1c)$$

$$n(t, 0) = 0, \quad c|_{\partial\Omega} = 0, \quad \mathcal{K}\nabla_x \phi \cdot \nu(\cdot)|_{\partial\Omega} = 0, \quad (1d)$$

$$n(t = 0, z) = n_0(z), \quad c(t = 0, x) = c_0(x). \quad (1e)$$

The growth-division dynamics for the tumor cells (1a) involves the (possibly size-dependent) growth rate $z \mapsto V(z) \geq 0$ and the cell division mechanism is embodied into the operator $Q(n)$. What is crucial for modeling purposes is the principle that cell-division does not change the total mass: the operator Q satisfies $\int_0^\infty zQ(n) dz = 0$. However, the total number of cells in the tumor increases since $\int_0^\infty Q(n) dz \geq 0$ (we refer the reader to [8] for further details). In what follows, we restrict to the mere symmetric binary division operator

$$Q(n)(t, z) = a(4n(t, 2z) - n(t, z)), \quad (2)$$

with $a > 0$ the division rate. Further relevant examples of division operators can be found in [15]. The boundary condition for n in (1d) means that no tumor cells are created with size 0.

In the right hand side of (1b), $(t, x) \mapsto R(t, x)$ stands for the space distribution of the influx rate of activated tumor antigen specific effector immune cells. It takes into account the sources of naive immune cells, namely T-cells and NK cells, that can be activated in the tumor microenvironment or in the draining lymph nodes into cells fighting the tumor. The rate of the activation process is supposed to be directly proportional to μ_1 . The Dirichlet boundary condition for c in (1d) means that the immune cells far from the tumor are non-activated. Immune cells are directed towards the tumor by a chemo-attractive potential ϕ , induced by the presence of the tumor cells. Through (1c), the strength of the signal is proportional to the total mass of the tumor, and it is shaped by a form function $x \mapsto \sigma(x)$. Finally, the activated immune cells are able to destroy tumor cells, as described by the death term in (1a)

$$m(c, n)(t, z) = \underbrace{\int_\Omega \delta(y)c(t, y) dy}_{:=\mu_c(t)} \times n(t, z), \quad (3)$$

where $\delta \geq 0$ is another form function. For the numerical experiments, we shall work with the Gaussian profiles

$$\delta(x) = \frac{A}{\theta\sqrt{2\pi}} \exp\left(-\frac{|x|^2}{2\theta^2}\right), \quad \sigma(x) = \frac{A_\sigma}{\theta_\sigma\sqrt{2\pi}} \exp\left(-\frac{|x|^2}{2\theta_\sigma^2}\right). \quad (4)$$

We refer the reader to [8] for further details and comments about the model.

Results

Identification of biological parameters

In order to go beyond the qualitative discussion of [8], the model should be challenged with biological data. The PDE system is governed by the set of parameters collected in **Table 1**: most parameter values were retrieved from previously published experimental results. We propose an estimation of the parameters R, a, V based on the experimental study performed in [16] where the development of chemically-induced cutaneous squamous cell carcinoma (cSCC) is investigated.

To estimate the parameter R , we used a simple linear regression, by using 34 data points from an in vivo experimental cutaneous squamous cell carcinoma (cSCC) tumor growth mouse model [16]: R is predicted from the “influx rate of effector immune cell”, denoted by Y and expressed in $cell_c \cdot day^{-1}$, given as a function, assumed to be linear, of the volume of the tumor μ_1 in μm^3 , see **Fig. 1-(a)**. The determination coefficient and the p-value are respectively, $r^2 = 0.705$ and $p = 2.84 \cdot 10^{-10}$, the slope of the regression line is $R = 7.92 \cdot 10^{-7}$. It is measured in $\frac{cell_c \cdot mm^{-3}}{\mu m^3} \cdot day^{-1}$ assuming homogeneity with respect to the unit mm^3 . **Table 1** gives the 95% confidence interval. This interval is quite small, but it already shows a sensitive impact of variations of this parameter; since the variability due to the biological model is likely important and we wished to investigate the impact of treatments that directly affect this parameter, we also made some simulations with a larger range of values (see for instance **Fig.6**)

We then determined the tumor growth parameters a and V . Neglecting the immune response, the tumor growth is driven by

$$\partial_t n + \partial_z(Vn) = Q(n). \quad (5)$$

As explained below, this leads to an exponential growth of the tumor mass, see [15, 29–31]. Let $t \mapsto \mu_0 = \int_0^\infty n(t, z) dz$ and $t \mapsto \mu_1(t) = \int_0^\infty zn(t, z) dz$. We thus get

$$\frac{d}{dt}\mu_0 = a\mu_0, \quad \frac{d}{dt}\mu_1 = V\mu_0. \quad (6)$$

We now aim at estimating the division rate a and the growth rate V from the experimental data, **Fig. 1-(b,c)**. We denote $\Theta = (a, V)$ the parameters to be identified. We have at hand some experimental noisy data $(Y_1^{(0)}, \dots, Y_n^{(0)})$, $(Y_1^{(1)}, \dots, Y_n^{(1)})$ representing respectively μ_0 and μ_1 at several times. Hence, we have

$$Y_i^{(j)} = \mu_{j,\Theta}(t_i) + \epsilon_i, \quad i \in \{1, \dots, n\}, \quad j \in \{0, 1\} \quad (7)$$

where $t \mapsto (\mu_{0,\Theta}, \mu_{1,\Theta})(t)$ stands for the solution of (6) defined with the parameters Θ . Forgetting for a while the discreteness of the observed data, the approach can be expressed

as a cost minimization problem where the cost function is defined by

$$C_\lambda^{(j)}(\Theta) = \int_0^T |\mu_{j,\Theta}(t) - Y^{(j)}(t)|^2 dt. \quad (8)$$

We finally set

$$\hat{\Theta} = \operatorname{argmin}\{C_\lambda^{(j)}(\Theta), \Theta = (a, V), a > 0, V > 0\}. \quad (9)$$

We fit the data that give the number of cells in the tumor and the volume of the tumor for several times by using a non-linear least square algorithm, the Levenberg-Marquardt algorithm [32], [33], **Fig. 1-(d,e)**.

Development of numerical methods predicting parameters of the equilibrium in immune-controlled tumors

Based on the space and size structured PDE model (1a)-(1e), we studied the equilibrium phase in immune-controlled tumors. We wished to predict, for given biological parameters, see **Table 1**, the total mass of the residual tumor and its size distribution. To this end, we developed specific numerical procedures based on the mathematical interpretation of the equilibrium.

Equilibrium states

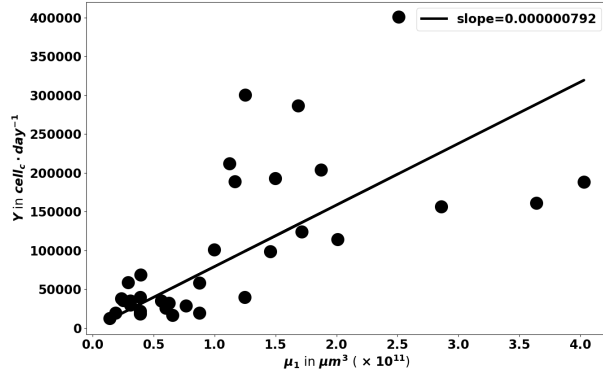
The definition of the equilibrium relies on the following arguments. The cell-division equation admits a positive eigenstate: in absence of immune response, see (5), the tumor population grows exponentially fast, with a rate $\lambda > 0$, and its size repartition obeys a certain profile \bar{N} . The equilibrium occurs when the immune response counterbalances the growth rate of this equation. To be more specific, we look for $\lambda > 0$ and a non negative function $z \geq 0 \mapsto \bar{N}(z)$ satisfying

$$\begin{cases} \partial_z(V\bar{N}) - Q(\bar{N}) + \lambda\bar{N} = 0 \text{ for } z \geq 0 \\ \bar{N}(0) = 0, \quad \bar{N}(z) > 0 \text{ for } z > 0, \quad \int_0^{+\infty} \bar{N}(z) dz = 1. \end{cases} \quad (10)$$

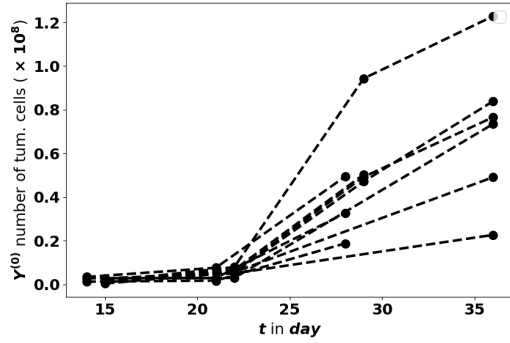
The existence-uniqueness of the eigenpair (λ, \bar{N}) can be found in [15, 29]. When the tumor does not interact with the immune system, the large time behavior is precisely driven by the eigenpair: the solution of (5) behaves like $n(t, z) \sim_{t \rightarrow \infty} \nu_0 e^{\lambda t} \bar{N}(z)$ where ν_0 is a constant determined by the initial condition, see [29, 30]. In the specific case where V is constant and Q is the binary division operator (2), we have $\lambda = a$ and the profile \bar{N} is explicitly known, [31, 34]. However, for general growth rates and division kernels the solution should be determined by numerical approximations.

Coming back to the coupled model, we infer that the equilibrium phase corresponds to the situation where the death rate precisely counterbalances the natural exponential growth of the tumor cell population. In other words, the equilibrium is defined by the stationary equation

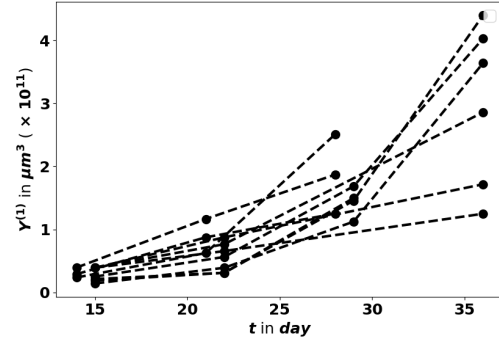
$$\gamma C - \nabla_x \cdot (D \nabla_x C) - \mu_1 \nabla_x \cdot (\chi C \nabla_x \Phi) = g(\mu_1) R, \quad C|_{\partial\Omega=0} = 0, \quad (11)$$



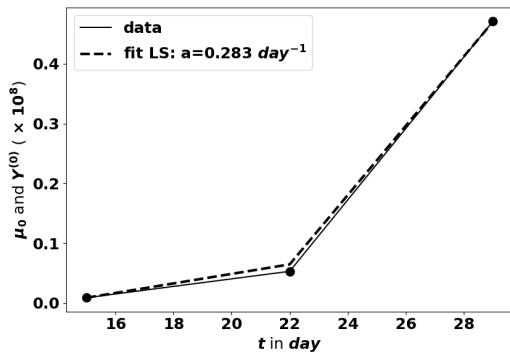
(a) influx rate of effector immune cell



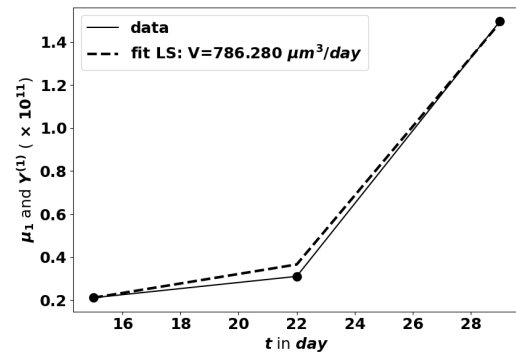
(b) tumor cell number



(c) tumor volume



(d) curve fit of tumor cell number



(e) curve fit of tumor volume

Figure 1. (a): Regression on the “influx rate of effector immune cell” Y (in $cell_c \cdot day^{-1}$) as a function of the tumor volume μ_1 in μm^3 (b) and (c): Tumor evolution kinetics from in vivo experimental cSCC tumor growth in mice. (d) and (e): Illustration of the estimation of the parameters a and V : $a = 0.283 \text{ day}^{-1}$ and $V = 786.280 \mu m^3 \cdot day^{-1}$ using 3 data points of a typical tumor evolution kinetic, from the dataset depicted in (b) and (c)

Symbol	Description	Value and unit	References
χ	chemotactic coefficient	$8.64 \times 10^1 - 8.64 \times 10^6$ $mm^2 \cdot mmol^{-1} \cdot day^{-1}$	(Macrophages) [17]
D	natural space diffusion coef. of the cytotoxic effector cells population	$8.64 \times 10^{-5} - 10^{-3} mm^2 \cdot day^{-1}$	(CD8 ⁺ T-cells) [18], [19]
R	the normal rate of influx of effector immune cells	$6.11 \times 10^{-7}, 9.74 \times 10^{-7}$ $\frac{cell \cdot mm^{-3}}{\mu m^3} \cdot day^{-1}$	estimated
γ	natural death rate of the tumor antigen-specific cytotoxic effector cells	$2 \times 10^{-2} - 1 day^{-1}$	[20], [21], [12], [22]
A	strength of the immune response	$2 - 57.6 cell^{-1} \cdot day^{-1}$	[23], [24], [25], [26]
\mathcal{K}	natural space diffusion of the attractive potential ϕ	$10^{-2} - 1 mm^2 \cdot day^{-1}$	[27], [19]
A_σ	strength of the chemical signal induced by each tumor cell	$5 \cdot 10^{-17} - 0.625 \times 10^{-16}$ $mmol \cdot \mu m^3 \cdot day^{-1}$	[28]
a	division rate of the tumor cells	$0.103 - 0.351 day^{-1}$	estimated
V	growth rate of the tumor cells	$308.526 - 2521.975 \mu m^3 \cdot day^{-1}$	estimated

Table 1. Key model parameters and their biophysical meaning

where Φ is the solution of

$$-\mathcal{K}\Delta_x \Phi = \sigma - \frac{1}{|\Omega|} \int_{\Omega} \sigma(y) dy,$$

endowed with the homogeneous Neumann boundary condition, together with the constraint

$$\int_{\Omega} \delta(x) C(x) dx = \lambda. \quad (12)$$

This can be interpreted as an implicit definition of the total mass μ_1 , to be the value such that the solution of the boundary value problem (11) satisfies (12). The existence of an equilibrium state defined in this way is rigorously justified in [8, Theorem 2]. **Fig. 2** illustrates how the equilibrium establishes in time: as time becomes large, the concentration of active immune cells in the neighborhood of the tumor tends to the eigenvalue of the cell-division equation, the total mass tends to a constant and the size distribution of tumor cells takes the profile of the corresponding eigenstate. This result has been obtained by using the lower bounds of the parameters in **Table 1** for the immune system and $(a, V) = (0.351, 713.608)$ for the tumor growth. We observe a non symmetric shape, peaked about a diameter of $13 \mu m$, which is consistent with

observational data reporting the mean size distribution of cancer cells [35].

Numerical experiments show that the model (1a)–(1e) is able to reproduce, in the long-time range, cancer-persistent equilibrium, but the features of the equilibrium, and its ability to establish, are highly sensitive to the parameters in **Table 1**. To discuss this issue further, we focus here on the mass at equilibrium considered as a critical quantity that evaluates the efficacy of the immune response. Indeed, it is known that a tumor gains in malignancy when its mass reaches certain thresholds [36, 37]. The smaller the tumor mass at equilibrium, the better the vital prognosis of the patient. In doing so, we do not consider transient states and time necessary for the equilibrium to establish (see **Fig. 4-(a-c)**).

The determination, on numerical grounds, of the equilibrium state relies on a two-step process. First, we compute the normalized eigenstate of the tumor cell equation, second, we find the tumor mass which makes the coupled death rate fit with the eigenvalue. To this end, we have developed a specific numerical approach.

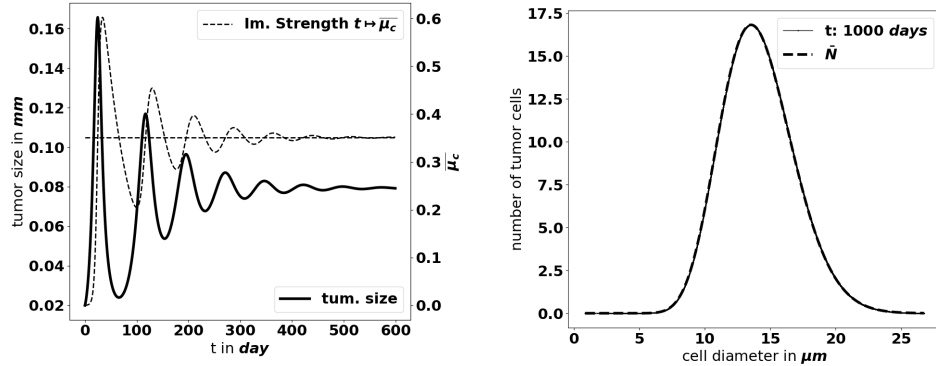


Figure 2. Left: Time evolution of the diameter of the tumor (bold black line) and concentration of active immune cells (dotted gray line). Right: Comparison of the tumor cell-size distribution at $t = 1000$ days with the positive eigenstate of the cell division equation (x-axis: size of the tumor cells, y-axis: number of tumor cells at the final time)

The eigen-elements of the growth-division equation

The numerical procedure is inspired from the spectral analysis of the equation: λ is found as the leading eigenvalue of a conveniently shifted version of the growth-division operator. In practice, we work with a problem where the size variable is both truncated and discretized. Hence, the problem recasts as finding the leading eigenvalue of a shifted version of the underlying matrix, which can be addressed by using the inverse power method [38, Section 1.2.5]. We refer the reader to [39, 40] for a thorough analysis of the approximation of eigenproblems for differential and integral operators, which provides a rigorous basis to this approach. It is also important to check a priori, based on the analysis of the equation [15], how large the shift should be, and that it remains independent on the numerical parameters, see Suppl. Material. For some specific fragmentation kernels and growth rates, the eigenpair (λ, N) is explicitly known, see [15]. We used these formula to validate the ability of the algorithm to find the expected values and profiles, see Suppl. Material.

Computation of the equilibrium mass

Having at hand the eigenvalue λ , we go back to the convection-diffusion equation (11) and the constraint (12) that determine implicitly the total mass μ_1 of the residual tumor. For a given value of μ_1 , we numerically solve (11) by using a finite volume scheme, see [8, Appendix C]. Then, we use the dichotomy algorithm to fit the constraint:

- The chemo-attractive potential Φ is computed once for all.
- Pick two reference values $0 < \mu_a < \mu_b$; the mass we are searching for is expected to belong to (μ_a, μ_b) .
- Set $\mu_1 = \frac{\mu_a + \mu_b}{2}$ and compute the associated solution C_{μ_1} of (11). Evaluate the discrete version of $I = \int \delta C_{\mu_1} dx - \lambda$.

- If $I < 0$, then replace μ_a by μ_1 , otherwise replace μ_b by μ_1 .
- We stop the algorithm when the relative error $\frac{\mu_b - \mu_a}{\mu_a} < \epsilon$ is small enough.

It is also possible to design an algorithm based on the Newton method. However, this approach is much more numerically demanding (it requires to solve more convection-diffusion equations) and does not provide better results.

For the evaluation of the residual mass, we do not know explicit solutions, even for the simplest model. Nevertheless, we can compare the results of the inverse power-dichotomy procedure that predicts the residual mass, to the large time simulations as performed in [8].

Therefore, we adopt the same framework as in [8]: the tumor is located at the origin of the computational domain Ω , which is the two-dimensional unit disk. We work with the lower bound of the parameters collected in **Table 1**. We compare the asymptotic value of the total mass μ_1^f given by the large time simulation of the evolution problem (and checking that the variation of the total mass has become negligible) to the total mass μ_1^{pd} predicted by the power-dichotomy procedure; let

$$E_{\mu_1} = \frac{|\mu_1^f - \mu_1^{pd}|}{\mu_1^f}.$$

The results for several cell division rates a are collected in **Table 2**: the numerical procedures finds the same equilibrium mass as the resolution of the evolution problem, which is another validation of the method.

Numerical simulations show how parameters influence equilibrium

The numerical methods were next used to assess how the parameters influence the equilibrium. In particular, we wish

a	$\mu_1^f (mm^3)$ at final time $T = 500$	$\mu_1^{pd} (mm^3)$	E_{μ_1}
0.103	$7.67271875 \times 10^{-5}$	$7.67271872 \times 10^{-5}$	4.10×10^{-9}
0.15	$1.11701535 \times 10^{-4}$	$1.11701543 \times 10^{-4}$	7.97×10^{-8}
0.20	$1.48924575 \times 10^{-4}$	$1.48924641 \times 10^{-4}$	4.40×10^{-7}
0.3	$2.23420663 \times 10^{-4}$	$2.23420562 \times 10^{-4}$	4.53×10^{-7}
0.351	$2.61368442 \times 10^{-4}$	$2.61367974 \times 10^{-4}$	1.80×10^{-6}

Table 2. Comparison of the large time tumor mass and the predicted tumor mass for several values of a

to assess the evolution of the tumor mass at equilibrium according to immune response and tumor growth parameters.

For the numerical simulations presented here, we thus work on the eigenproblem (10) and on the constrained system (11)-(12). Unless precisely stated, the immune response parameters are fixed to the lower bounds in **Table 1**. The tumor growth parameters are set to $a = 0.3 \text{ day}^{-1}$ and $V = 469.545 \mu m^3 \cdot \text{day}^{-1}$. When necessary, the initial values of the unknowns are respectively $\mu_0(0) = 1 \text{ cell}_n$, $\mu_1(0) = 4188 \mu m^3$, $c(0, x) = 0$.

The main features of the solutions follow the observations made in [8], which were performed with arbitrary “academic” values for the parameters. We observe that $\int_{\Omega} \delta(y) c(t, y) dy$ tends to the division rate a , which in this case corresponds to the leading eigenvalue of the cell-division equation. It is remarkable that the predicted diameter of the tumor at equilibrium — see **Fig. 2** — is significantly below modern clinical PET scanners resolution limit, which could detect tumors with a diameter larger than 7 mm [41]. This is consistent with the standard expectations about the equilibrium phase [7], but, of course, it makes difficult further comparison of the prediction with data.

The aggressiveness of the tumor is characterized by the division rate, the variations of which impact the size of the tumor at equilibrium: the larger a , the larger the residual tumor, see **Fig. 3-(a)**. Increasing the immune strength A increases the efficacy of the immune response, reducing the size of the residual tumor see **Fig. 3-(b)**. Similarly, increasing the mean rate of influx of effector immune cells in the tumor microenvironment R , decreases the tumor size at equilibrium, see **Fig. 3-(c)**. On the contrary, increasing the death rate of the immune cells γ reduces the efficacy of the immune response and increases the equilibrium tumor size see **Fig. 3-(d)**.

Moreover, as mentioned above, not only the parameters determine the equilibrium mass, but they also impact how the equilibrium establishes. **Fig. 4-(a-c)** shows what happens by making the tumor cell division rate a vary. There are more oscillations along time, with larger amplitude, as a increases. Similar observations can be made when reducing the strength of the immune system A (likely out of its realistic range), see **Fig 4-(d-f)**. The smaller A , the weaker the damping of the oscillations and the longer the periods. We notice that the decay of the maximal tumor radius holds at a polynomial

rate. In extreme situations, the equilibrium does not establish on reasonable observation times, and the evolution can be confounded with a periodic alternance of growing and remission phases. Such scenario illustrates that the relevance of the equilibrium can be questionable depending on the value of the parameters. In what follows, we focus on the details of the equilibrium itself, rather than on the transient states.

Global sensitivity analysis on the equilibrium mass identifies the key parameters to target in cancer therapy

Since the equilibrium state can be computed for a reduced numerical cost (it takes about 1/4 of a second on a standard laptop), we can perform a large number of simulations, sampling the range of the parameters. This allows us to discuss in further details the influence of the parameters on the residual mass and, by means of a global sensitivity analysis, to make a hierarchy appear according to the influence of the parameters on this criterion. Ultimately, this study can help in proposing treatments that target the most influential parameters.

Details on the applied methods for the sensitivity analysis can be found in the Suppl. Material. Among the parameters, we distinguish:

- the tumor cell division rate a which drives the tumor aggressiveness,
- the efficacy of the immune system, governed by the mean influx rate of activated effector immune cells R , the strength of the immune response A , the chemotactic sensitivity χ , the death rate γ of the immune cells, and the strength of the chemical signal induced by each tumor cell A_σ
- environmental parameters such as the diffusion coefficients D (for the immune cells) and \mathcal{K} (for the chemokine concentration).

We assume that the input parameters are independent random variables. Due to the lack of knowledge on the specific distribution of these parameters and according to the constraints on the parameter bounds (**Table 1**), the most suitable probability distribution is the one which maximizes the continuous entropy ([42]), more precisely, the uniform distribution. Therefore, the uncertainty in the parameter values is represented by uniform distributions $\mathcal{U}(p_{min}, p_{max})$ where

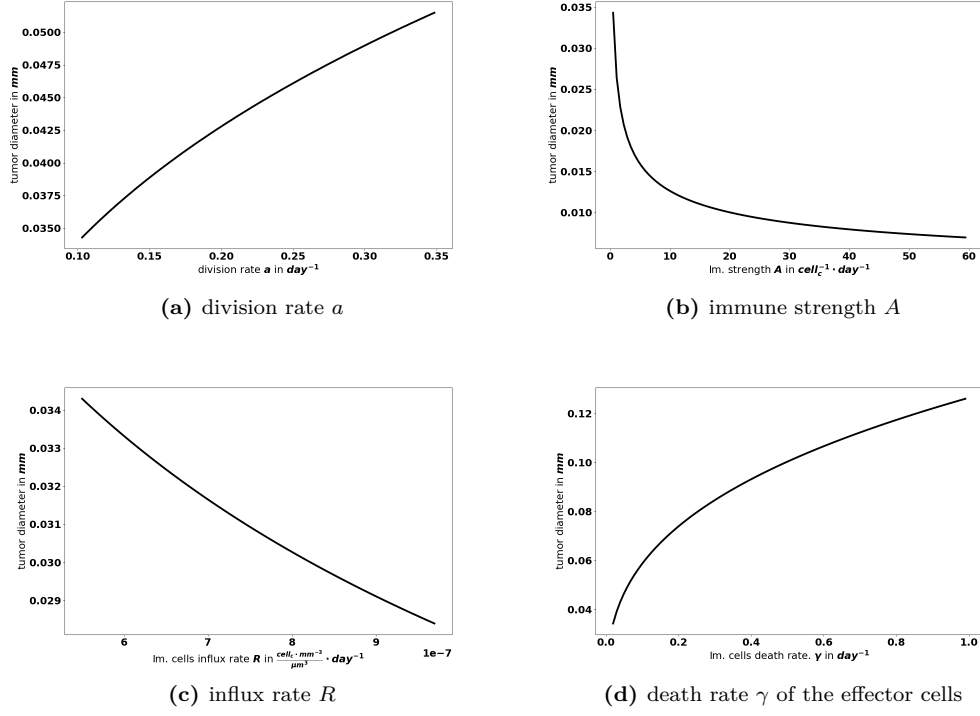


Figure 3. Evolution of the tumor diameter at equilibrium, with respect to the division rate a , the strength of the effector immune cells A , the influx rate of effector immune cells R , the natural death rate γ of the effector cells

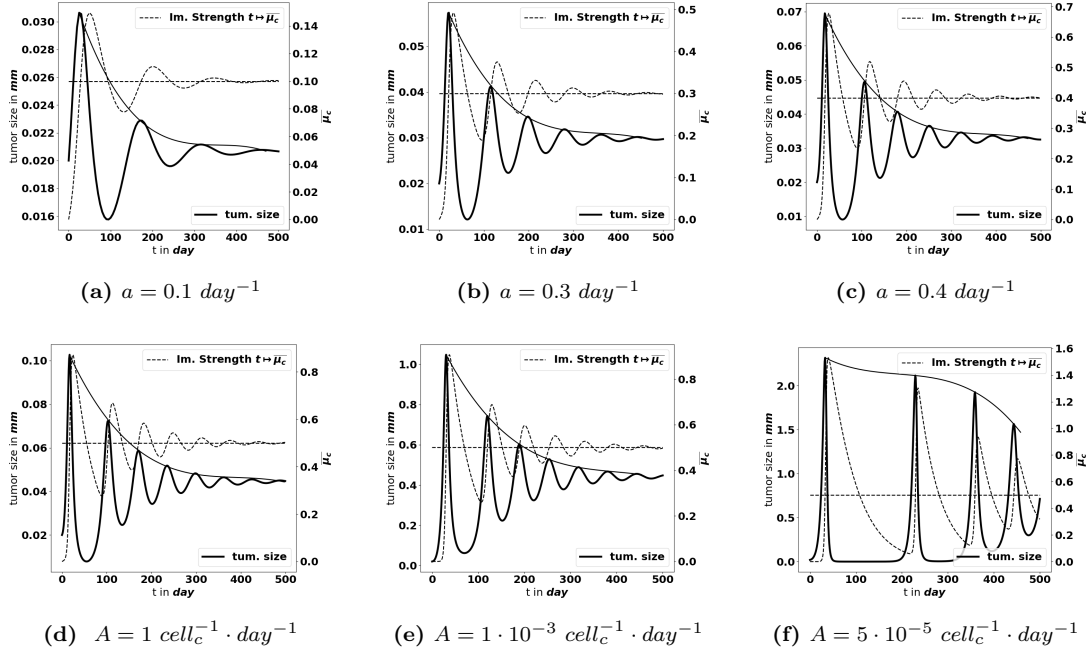


Figure 4. Large-time simulation of the PDE system: evolution of the tumor diameter (bold black line, left axis), and of the concentration of immune cells $\bar{\mu}_c$ (dotted grey line, right axis), for several values of the division rate a (top) and for several values of the immune strength A (bottom). The equilibrium needs more time to establish as the strength of the immune system decreases

p_{min} and p_{max} are respectively the lower and upper bound of each uncertain input parameter (see **Table 1**). In what follows, the total mass at equilibrium, μ_1 , given by the power-dichotomy algorithm, is seen as a function of the uncertain parameters:

$$\mu_1 = f(a, A, R, \chi, D, A_\sigma, \gamma, \mathcal{K}). \quad (13)$$

To measure how the total variance of the output μ_1 of the algorithm is influenced by some subsets $i_1 \dots i_p$ of the input parameters $i_1 \dots i_k$ ($k \geq p$ being the number of uncertain input parameters), we compute the so-called Sobol's sensitivity indices. The total effect of a specific input parameter i is evaluated by the total sensitivity index $S_T^{(i)}$, the sum of the sensitivity indices which contain the parameter i . (Details on the computed Sobol indices can be found in Suppl. Material). The computation of these indices is usually based on a Monte Carlo (MC) method (see [43, 44]) which requires a large number of evaluations of the model due to its slow convergence rate ($O(1/\sqrt{N})$ where N is the size of the experimental sample). To reduce the number of model evaluations, we use instead the so-called generalized Polynomial Chaos (gPC) method (see [45]). The backbone of the method is based on building a surrogate of the original model by decomposing the quantity of interest on a basis of orthonormal polynomials depending on the distribution of the uncertain input parameters $\theta(\omega) = (a, A, R, \chi, D, A_\sigma, \gamma, \mathcal{K})$, where ω represents an element of the set of possible outcomes. Further details on the method can be found in [46]. For uniform distributions, the most suitable orthonormal polynomial basis is the Legendre polynomials. The analysis of the distribution of μ_1 after a suitable sampling of the parameters space indicates that μ_1 follows a log-normal distribution. This distribution is not uniquely determined by its moments (the Hamburger moment problem) and consequently cannot be expanded in a gPC (see [47]). Based on this observation, to obtain a better convergence in the mean square sense, we apply the gPC algorithm on the natural logarithm of the output μ_1 . Typically, $\ln(\mu_1)$ is decomposed as follows:

$$\ln(\mu_1(\omega)) = \sum_{\alpha \in \mathcal{I}_{k,p}} q_\alpha L_\alpha(\theta(\omega)) + \varepsilon, \quad (14)$$

where ε corresponds to the approximation error, $\mathcal{I}_{k,p} = \{\alpha \in \mathbb{N}^k : \sum_{i=1}^k \alpha_i \leq p\}$ and p represents the highest degree of the expansion. Hence, the dimension of the polynomial basis is given by $\frac{(k+p)!}{k!p!}$. We reduce the number of model evaluations to 642 runs by constraining also the parameters interaction order to 2. For our purpose, a degree $p = 5$ gives a better fit (see **Fig. 5-Top**) to the original model and the goodness of fit of the gPC algorithm is measured by a Leave One Out Cross Validation (LOOCV) technique [48]. The resulting LOO error indicates 0.4% prediction error. The Sobol's sensitivity indices are then computed from the exponential of the surrogate model (14) by using Monte Carlo simulations

combined with a careful space-filling sampling of the parameters space (see [43, 49]). For the computations, a sample with $N = 1.8 \times 10^6$ points has been used in order to get stable second order Sobol indices. Indeed, the sensitivity indices that are needed to discriminate the impact of the input parameters are the first and total Sobol' sensitivity indices. Here, the analysis revealed a significant difference between some first order Sobol' indices and their corresponding total Sobol indices, which indicated the importance of computing also the second order Sobol' indices.

It is important to stress that the obtained results, and the associated conclusions, could be highly dependent on the range of the parameter values. This observation makes the measurement / estimation of the parameters a crucial issue which can be dependent on the type of cancer analyzed.

Efficacy of the immune response The first order Sobol indices represented in **Fig. 5-bottom-left** indicate that the parameters which impact the most the variability of the immune-controlled tumor mass at equilibrium are respectively,

- the strength of the lethal action of the immune cells on the tumor cells A ,
- the natural death rate γ of the effector immune cells,
- the division rate a of the tumor cells,
- the influx rate of activated effector immune cells into the tumor microenvironment R .

This is consistent with the observations made from the numerical experiments above and in [8]: the immune response is enhanced by increasing either A or R , and decreasing γ . Surprisingly, the chemotactic sensitivity χ , like the strength of the chemical signal induced by each tumor cell A_σ , the space diffusion coefficient of the effector immune cells D and the diffusion coefficient of the chemokines \mathcal{K} , have a negligible influence on the immune-controlled tumor mass, see **Fig. 5-bottom-left**, whether individually or in combination with other parameters. This result can be explained by the fact that despite the capacity of the cells of the immune system to infiltrate the tumor, this ability has a reduced effect when these cells are not able to effectively kill the tumor cells.

The second order Sobol' indices indicate that the leading interactions are the pairs (A, γ) , (a, A) , (a, γ) and (A, R) . Accordingly, in order to enhance the immune response, an efficient strategy can be to act simultaneously on the immune strength A together with the natural death rate γ or together with tumor division rate a . Increasing the influx rate of activated effector immune cells into the tumor microenvironment R , by enhancing the activation / recruitment processes leading to the conversion of naive immune cells into tumor antigen specific effector immune cells, can also be efficient when combined with an action on A .

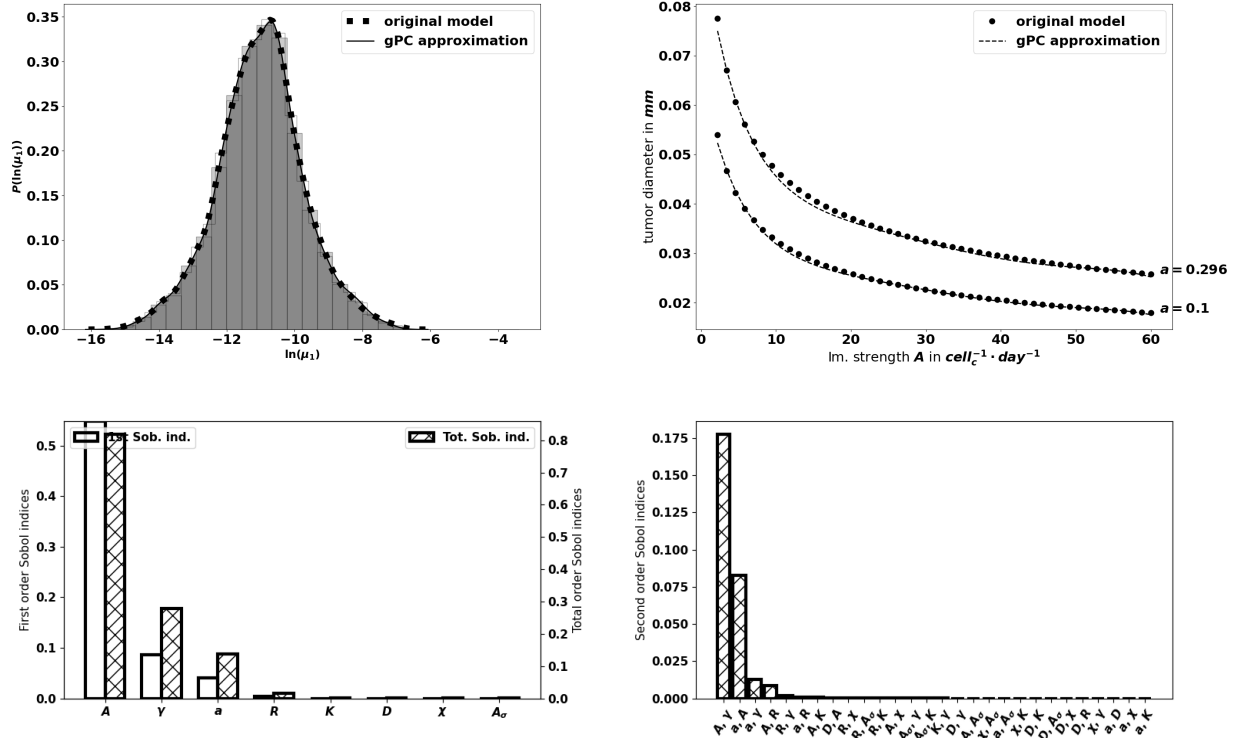


Figure 5. Top-Left: comparison between the pdf of $\ln(\mu_1)$ from the gPC approximation and the pdf from the original model. Top-Right: Comparison between the value of μ_1 generated by the power-dichotomy algorithm and the gPC approximation. Bottom-Left: First (empty) and total (dashed) order Sobol indices for μ_1 . Bottom-Right: Second order Sobol indices for μ_1

The tumor aggressiveness The tumor aggressiveness is mainly described by the cell division rate a . The first order Sobol indice indicates that a influences significantly the tumor mass at equilibrium, and we observe that the total Sobol index of a is higher than the individual one. This indicates that this parameter has strong interactions with the others. By taking a look at **Fig. 5**-bottom-right we remark that a interacts significantly with the parameters A, γ . However, the most significant interaction is the one with A . This is consistent with recent successes of combined therapies targeting tumor and immune cells [50].

Towards optimized treatments Because equilibrium state can be computed for a reduced numerical cost, it allows a large number of simulation to be performed in a minimal time, so that an extensive sampling of the range of the parameters can be tested. The flexibility of the numerical simulations provides valuable tools to assess the efficiency of a variety of therapeutic strategies.

Fig. 6 illustrates how the equilibrium mass is impacted when combining variations of two parameters, namely the immune strength A combined to the tumor cell division rate a , the mean rate of influx of effector immune cells R or the death rate of effector immune cells γ ; and the tumor cell division rate a with the death rate γ . Interestingly, a reduction of the tumor mass at equilibrium can be obtained significantly more easily by acting on two parameters than on a single one. For

instance, reducing the tumor cell division rate a from 0.35 to 0.1 cannot reduce the diameter of the tumor below .025 mm, with $A = 1$; while the final size is always smaller when $A = 3.95$. This observation highlights the interest of combined treatments having such complementary actions. The interest is two-fold: either smaller residual tumors can be obtained by pairing two actions, or the same final tumor size can be obtained with a combined treatment having less toxicity than a mono-therapy.

Conclusion and Discussion

Controlling parameters that maintain cancer-immune equilibrium is key to the successful development of future cancer therapies. To understand how equilibrium establishes and how it is influenced by immune, environmental and tumor-related parameters, we evaluate the tumor mass which tends to a constant at equilibrium. In this study, we make use of the space and size structured mathematical model developed in [8] to provide innovative, efficient methods to predict, at low numerical cost, the residual tumor mass at equilibrium. By means of numerical simulations and global sensitivity analysis, we identify the elimination rate A of tumor cells by immune cells as the most influential factor. Therefore, the most efficient therapeutic strategy is to act primarily on the immune system rather than on the tumor itself. We also demonstrate the need to develop combined cancer treatments,

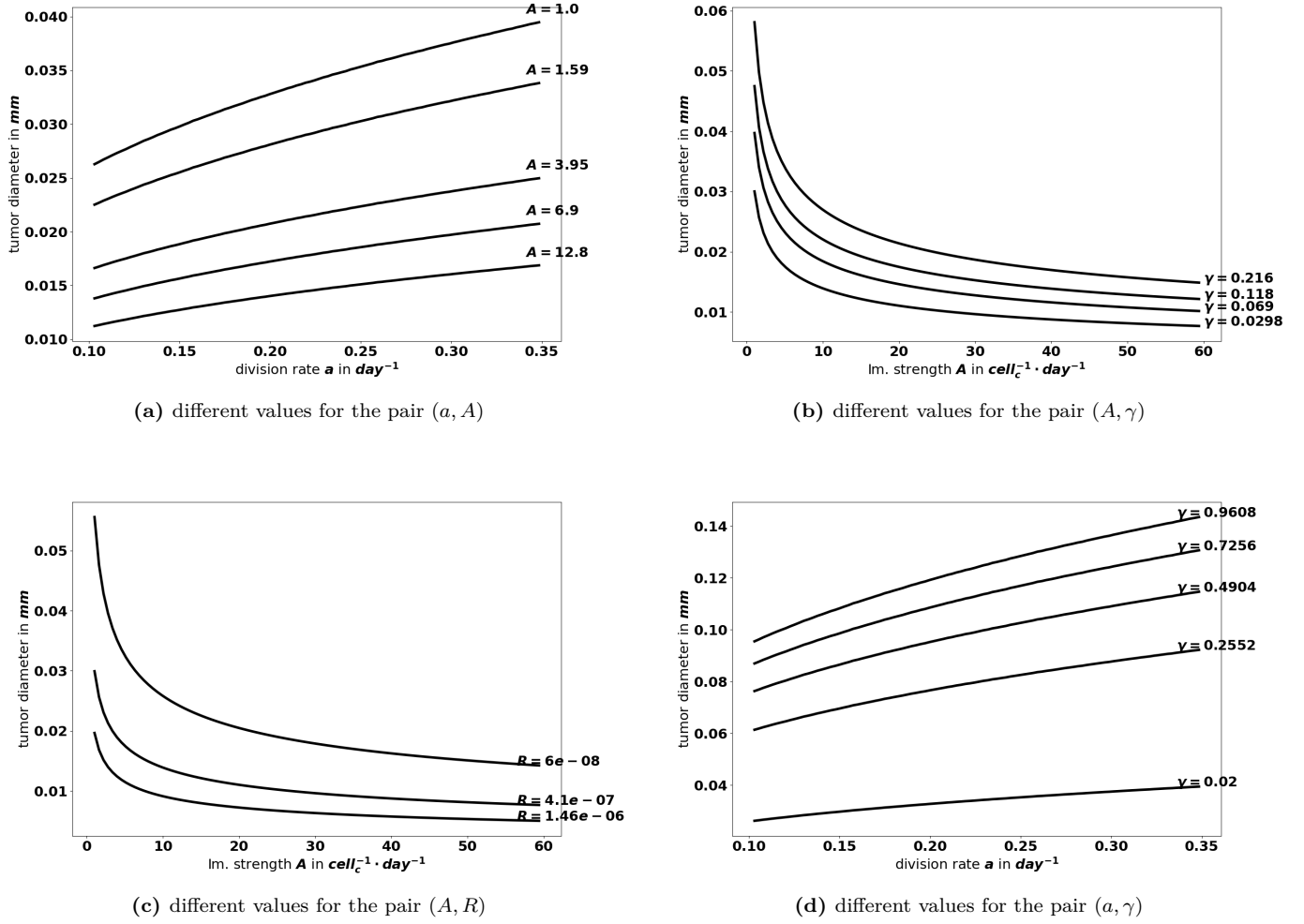


Figure 6. Evolution of the tumor diameter at equilibrium, with respect to the division rate a for several values of the immune strength A (a), with respect to the immune strength A for several values of the death rate γ (b), with respect to the immune strength A for several values of the influx rate of effector immune cells R (c), and with respect to the division rate a for several values of the death rate γ (d).

boosting the immune capacity to kill tumor cells (increase A), reducing natural death rate of effector immune cells (decrease γ), boosting the conversion into efficient immune cells (increase R) and reducing the ability of tumor cells to divide (decrease a). The combination of such approaches definitely outperforms the performances of a single action; it permits to maintain the tumor in a long-lasting equilibrium state, far below measurement capabilities.

Generally, therapeutic strategies are designed to target preformed, macroscopic cancers. Indeed, patients are diagnosed once their tumor is established and measurable, thus at the escape phase of the cancer immunoediting process [1]. The goal of successful treatments is to revert to the equilibrium phase and ultimately to tumor elimination. Experimental and clinical evidence indicate that equilibrium exists but it is difficult to measure, being below detection limit. It is regarded as “a tumor mass dormancy” when the rate of cancer cell proliferation matches their rate of elimination by immune

cells. In human, cancer recurrence after therapy and long periods of remission or detection of low number of tumor cells in remission phases are suggestive of such equilibrium phase. Mathematical models can also be used to provide evidence of such state. The system of partial differential equations proposed in [8] is precisely intended to describe the earliest stages of immune control of tumor growth. Remarkably, while being in the most favorable condition, only taking into account the tumor antigen-specific cytotoxic immune cells and no immunosuppressive mechanisms, the model reproduces the formation of an equilibrium phase with maintenance of residual tumor cells rather than their complete elimination. Besides suggesting that elimination may be difficult to reach, this finding also brings out the role of leading parameters that shape the equilibrium features and opens new perspectives to elaborate cancer therapy strategies that reach this state of equilibrium.

To decipher tumor-immune system dynamics leading to

equilibrium state, we have developed here computational tools. The total mass of the tumor is a critical criterion of the equilibrium and was used to predict parameters that contribute the most to the establishment of the equilibrium. By means of global sensitivity analysis, we identified four parameters that affect the most the variability of the immune-controlled tumor mass. Three of them are related to immune cells, A , R and γ and one to tumor cells, a . Moreover, the influence of the leading parameters is significantly increased when they are paired. This observation validates the development of combined therapeutic treatments which would be more efficient at reducing tumor growth and reduce toxicity. Because the pair (a, A) is among the most influential, we predict that a combination of drugs enhancing anti-tumor immune response with drugs diminishing tumor aggressiveness will be the most efficient. This is confirmed by the clinical benefit obtained when chemotherapies reducing the tumor cell division rate a are combined with immunotherapies increasing A and R , [50]. The parameter A which governs the efficacy of the immune system to eliminate tumor cells, is the most influential. This finding correlates with the observation that “hot” tumors infiltrated with immune cells have better prognostic than “cold” tumors [51] and that the immune cells with the strongest positive impact on patient’s survival are the cytotoxic $CD8^+$ T cells [52]. It is also in line with the success of immune checkpoint inhibitors which revert immune tolerance triggered by chronic activation and upregulation of exhaustion markers on effector T and NK cells, thus not only increasing the parameter A but also R [53]. The leading role of the parameter A is also validated by experimental studies and clinical trials, including adoptive transfer of CAR-T and CAR-NK cells engineered to attack cancer cells, immunomodulating antibody therapies or cancer vaccines which boost the anti-tumor immune response [50, 54, 55]. Finally, our finding that the parameter γ is highly influential is validated by the administration of cytokines that stimulate and increase effector T and NK cell survival which are efficient at controlling tumor growth [55]. Thus, altogether, these experimental and clinical data validate the numerical method.

Interestingly, besides the dominant role of the parameter A , only two additional parameters related to immune cells R , γ seems to have an influence on the tumor mass at equilibrium. These data predict that to enhance the immune response, it is more efficient to increase the rate of influx and conversion of naive immune cells into effector cells (parameter R) or to increase the lifespan of immune effectors (parameter γ) than to increase chemotaxis as a whole (parameters χ , A_σ , \mathcal{K}). The lack of influence of chemotaxis emphasizes that the localization of immune cells within tumors is necessary but not sufficient. Indeed, the leading influence of the parameters A , R , γ stresses the importance of having functional immune cells infiltrating tumors. Overcoming immune suppression is therefore highly relevant in therapeutic strategies.

In conclusion, clinical trials have been undertaken quite often on assumptions from acquired knowledge on tumor development and immune responses to cancer cells, but without tools to help the decision-making. The numerical methods developed here provide valuable hints for the design and the optimization of anti-tumor therapies. The approach is validated by clinical evidence obtained so far. By adapting the range of the parameters to the biological values, one can more precisely adapt the therapeutic strategies to specific types of tumors. We thus conclude that mathematical modelling combined with numerical validation provide valuable information that could contribute to better stratify the patients eligible for treatments and consequently save time and lives. In addition, it could also help to decrease the burden of treatment cost providing hints on optimized therapeutic strategies.

Materials and Methods

Mice FVB/N wild-type (WT) mice (Charles River Laboratories, St Germain Nuelles, France) were bred and housed in specific-pathogen-free conditions. Experiments were performed using 6-7 week-old female FVB/N, in compliance with institutional guidelines and have been approved by the regional committee for animal experimentation (reference MESR 2016112515599520; CIEPAL, Nice Côte d’Azur, France).

In vivo tumor growth mSCC38 tumor cell line was established from DMBA/PMA induced sSCCs and maintained in DMEM (Gibco-ThermoFisher Scientific, Courtaboeuf, France) supplemented with 10% heat-inactivated fetal bovine serum (FBS) (GE Healthcare, Chicago, Illinois, USA) penicillin (100 U/ml) and streptomycin (100 $\mu g/ml$) (Gibco-ThermoFisher Scientific, Courtaboeuf, France). 5×10^5 mSCC38 were intradermally injected in anesthetized mice after dorsal skin shaving. Tumor volume was measured manually using a ruler and calculated according to the ellipsoid formula: Volume = Length (mm) \times Width (mm) \times Height (mm) $\times \pi/6$.

Tissue preparation and cell count mSCC38 were excised and enzymatically treated twice with collagenase IV (1 mg/ml) (Sigma-Aldrich, St Quentin Fallavier, France), and DNase I (0.2 mg/ml) (Roche Diagnostic, Meylan, France) for 20 minutes at 37° C. Total cell count was obtained on a Casy cell counter (Ovni Life Science, Bremen, Germany). Immune cell count was determined from flow cytometry analysis. Briefly, cell suspensions were incubated with anti-CD16/32 (2.4G2) to block Fc receptors and stained with anti-CD45 (30-F11)-BV510 antibody and the 7-Aminoactinomycin D (7-AAD) to identify live immune cells (BD Biosciences, Le Pont de Claix, France). Samples were acquired on a BD LSR Fortessa and analyzed with DIVA V8

and FlowJo V10 software (BD Biosciences, Le Pont de Claix, France).

Mathematical and statistical analysis Computations were realized in `Python` and we made use of dedicated libraries, in particular the `gmsh` library for the computational domain mesh generation, the packages `optimize` (for the the optimization methods using the Levenberg-Marquard mean square algorithm; similar results have been obtained with the CMA-ES algorithm of the library `cma`) from the library `scipy`, the library `Pygpc` for the generalized Polynomial Chaos approximation [56] and the library `Salib` for the sensitivity analysis [57].

Authors' Contributions

Conception and design: K. Atsou, V. M. Braud, T. Goudon

Development of methodology: K. Atsou, V. M. Braud, T. Goudon

Acquisition of data (provided animals, acquired and managed patients, provided facilities, etc.): F. Anjuère, V. M. Braud, S. Khou

Analysis and interpretation of data (e.g., statistical analysis, biostatistics, computational analysis): K. Atsou, V. M. Braud, T. Goudon

Writing, review, and/or revision of the manuscript: K. Atsou, F. Anjuère, V. M. Braud, T. Goudon

Study supervision: F. Anjuère, V. M. Braud, T. Goudon

Acknowledgements

The authors acknowledge the support of UCAnCer, an incentive Université Côte d'Azur network, which has permitted and encouraged this collaboration. We thank the IPMC's animal house and Imaging/Flow cytometry core facilities for technical support. This work was supported by the French Government (National Research Agency, ANR) through the "Investments for the Future" programs LABEX SIGNALIFE ANR-11-LABX-0028 and IDEX UCAJedi ANR-15-IDEX-01.

Code availability

Codes are available at the URL <https://github.com/atsoukevin93/tumorgrowth>

Data availability

Numerical data necessary to replicate the results of the paper are available at the URL <https://github.com/atsoukevin93/tumorgrowth>

References

- [1] Dunn, G. P., Bruce, A. T., Ikeda, H., Old, L. J. & Schreiber, R. D. Cancer immunoediting: from immunosurveillance to tumor escape. *Nat. Immunol.* **3**, 991–998 (2002).

- [2] Boon, T., Coulie, P. G., den Eynde, B. J. V. & van der Bruggen, P. Human T-cell responses against melanoma. *Annual Review of Immunology* **24**, 175–208 (2006). URL <https://doi.org/10.1146/annurev.immunol.24.021605.090733>. PMID: 16551247, <https://doi.org/10.1146/annurev.immunol.24.021605.090733>.
- [3] Dranoff, G. Cytokines in cancer pathogenesis and cancer therapy. *Nature Reviews Cancer* **4**, 11–22 (2004).
- [4] Rabinovich, G. A., Gabrilovich, D. & Sotomayor, E. M. Immunosuppressive strategies that are mediated by tumor cells. *Ann. Rev. Immunol.* **25**, 267–296 (2007). URL <https://doi.org/10.1146/annurev.immunol.25.022106.141609>. PMID: 17134371, <https://doi.org/10.1146/annurev.immunol.25.022106.141609>.
- [5] Smyth, M. J., Godfrey, D. I. & Trapani, J. A. A fresh look at tumor immunosurveillance and immunotherapy. *Nat. Immunol.* **2**, 293–299 (2001).
- [6] Whiteside, T. L. Immune suppression in cancer: Effects on immune cells, mechanisms and future therapeutic intervention. *Seminars in Cancer Biology* **16**, 3–15 (2006). URL <http://www.sciencedirect.com/science/article/pii/S1044579X0500060X>. The Inflammation-Cancer Linkage: A Double-Edged Sword?
- [7] Koebel, C. M. *et al.* Adaptive immunity maintains occult cancer in an equilibrium state. *Nature* **450**, 903–908 (2007).
- [8] Atsou, K., Anjuère, F., Braud, V. M. & Goudon, T. A size and space structured model describing interactions of tumor cells with immune cells reveals cancer persistent equilibrium states in tumorigenesis. *J. Theor. Biol.* **490**, 110163 (2020).
- [9] Kirschner, D. E. & Panetta, J. C. Modeling immunotherapy of the tumor-immune interaction. *J. Math. Biol.* **37**, 235–252 (1998).
- [10] Konstorum, A., Vella, A. T., Adler, A. J. & Laubacher, R. C. Addressing current challenges in cancer immunotherapy with mathematical and computational modelling. *J. Royal Soc. Interface* **14**, # 20170150 (2017). 1706.01989.
- [11] Lai, X. *et al.* Modeling combination therapy for breast cancer with BET and immune checkpoint inhibitors. *Proc. Nat. Acad. Sc.* **115**, 5534–5539 (2018).
- [12] de Pillis, L. G., Radunskaya, A. E. & Wiseman, C. L. A validated mathematical model of cell-mediated immune response to tumor growth. *Cancer Res.* **65**, 7950–7958 (2005). URL <http://cancerres.aacrjournals.org/content/65/17/7950>. <http://cancerres.aacrjournals.org/content/65/17/7950.full.pdf>.

- [13] Eftimie, R., Bramson, J. L. & Earn, D. J. D. Interactions between the immune system and cancer: A brief review of non-spatial mathematical models. *Bull. Math. Biol.* **73**, 2–32 (2011). URL <https://doi.org/10.1007/s11538-010-9526-3>.
- [14] Wilkie, K. P. & Hahnfeldt, P. Modeling the dichotomy of the immune response to cancer: Cytotoxic effects and tumor-promoting inflammation. *Bull. Math. Biol.* **79**, 1426–1448 (2017).
- [15] Doumic-Jauffret, M. & Gabriel, P. Eigenelements of a general aggregation-fragmentation model. *Math. Models Methods Appl. Sci.* **20**, 757–783 (2010). URL <https://doi.org/10.1142/S021820251000443X>.
- [16] Khou, S. *et al.* Tumor-associated neutrophils dampen adaptive immunity and promote cutaneous squamous cell carcinoma development. *Cancers* **10-12**, E1860 (2020).
- [17] Farrell, B. E., Daniele, R. P. & Lauffenburger, D. A. Quantitative relationships between single-cell and cell-population model parameters for chemosensory migration responses of alveolar macrophages to C5a. *Cell Motility* **16**, 279–293 (1990). URL <https://onlinelibrary.wiley.com/doi/abs/10.1002/cm.970160407>. <https://onlinelibrary.wiley.com/doi/pdf/10.1002/cm.970160407>.
- [18] Friedman, A. & Hao, W. The role of exosomes in pancreatic cancer microenvironment. *Bull. Math. Biol.* **80**, 1111–1133 (2018). URL <https://doi.org/10.1007/s11538-017-0254-9>.
- [19] Matzavinos, A., Chaplain, M. A. J. & Kuznetsov, V. A. Mathematical modelling of the spatio-temporal response of cytotoxic *T*-lymphocytes to a solid tumour. *Math. Medicine and Biology* **21**, 1–34 (2004).
- [20] Yates, A. & Callard, R. Cell death and the maintenance of immunological memory. *Disc. Cont. Dyn. Syst.-B* **1**, 43–59 (2001).
- [21] Chaplain, M. A., Kuznetsov, V. A., James, Z. H., Davidson, F. & Stepanova, L. A. Spatio-temporal dynamics of the immune system response to cancer. In Horn, M. A., Gieri, S. & Webb, G. F. (eds.) *Mathematical models in medical and health science* (Vanderbilt University Press, 1998). International Conference on Mathematical Models in Medical and Health Sciences.
- [22] Kuznetsov, V. A., Makalkin, I. A., Taylor, M. A. & Perelson, A. S. Nonlinear dynamics of immunogenic tumors: Parameter estimation and global bifurcation analysis. *Bull. Math. Biol.* **56**, 295–321 (1994). URL <https://doi.org/10.1007/BF02460644>.
- [23] Beck, R. J., Slagter, M. & Beltman, J. B. Contact-dependent killing by cytotoxic *T* lymphocytes is insufficient for EL4 tumor regression in vivo. *Cancer Research* **79**, 3406–3416 (2019). URL <https://cancerres.aacrjournals.org/content/79/13/3406>. <https://cancerres.aacrjournals.org/content/79/13/3406.full.pdf>.
- [24] Cazaux, M. *et al.* Single-cell imaging of CAR *T*-cell activity in vivo reveals extensive functional and anatomical heterogeneity. *J. Experimental Medicine* **216**, 1038–1049 (2019).
- [25] Hanson, H. L. . *et al.* Eradication of established tumors by *CD8+* *T*-cell adoptive immunotherapy. *Cell Press* **13**, 265–276 (2000).
- [26] Nolz, J. C. & Hill, A. B. Strength in numbers: Visualizing CTL-mediated killing in vivo. *Immunity* **44**, 207–208 (2016). URL <http://www.sciencedirect.com/science/article/pii/S1074761316300139>.
- [27] Kwok, C. S., Cole, S. E. & Liao, S.-K. Uptake kinetics of monoclonal antibodies by human malignant melanoma multicell spheroids. *Cancer Res.* **48**, 1856–1863 (1988). URL <https://cancerres.aacrjournals.org/content/48/7/1856>. <https://cancerres.aacrjournals.org/content/48/7/1856.full.pdf>.
- [28] Cairns, C. M. *et al.* Lymphotactin Expression by Engineered Myeloma Cells Drives Tumor Regression: Mediation by *CD4+* and *CD8+* *T*-Cells and Neutrophils Expressing *XCR1* Receptor. *J. Immun.* **167**, 57–65 (2001).
- [29] Michel, P. Existence of a solution to the cell division eigenproblem. *Models Math. Meth. App. Sci.* **16**, 1125–1153 (2006).
- [30] Michel, P., Mischler, S. & Perthame, B. General relative entropy inequality: an illustration on growth models. *J. Math. Pures et Appl.* **84**, 1235–1260 (2005).
- [31] Perthame, B. & Ryzhik, L. Exponential decay for the fragmentation or cell-division equation. *J. Differ. Eq.* **210**, 155–177 (2005).
- [32] Moré, J. J. The Levenberg-Marquardt algorithm: Implementation and theory. In Watson, G. A. (ed.) *Numerical Analysis*, 105–116 (Springer Berlin Heidelberg, Berlin, Heidelberg, 1978).
- [33] Ramadasan, D., Chevaldonné, M. & Chateau, T. LMA: A generic and efficient implementation of the Levenberg-Marquardt algorithm. *Software: Practice and Experience* **47**, 1707–1727 (2017).
- [34] Baccelli, F., McDonald, D. & Reynier, J. A mean field model for multiple TCP connections through a buffer

- implementing RED. *Performance Evaluation* **49**, 77–97 (2002).
- [35] Shashni, B. *et al.* Size-based differentiation of cancer and normal cells by a particle size analyzer assisted by a cell-recognition pc software. *Biological and Pharmaceutical Bulletin* **41**, 487–503 (2018).
- [36] Faget, J. *et al.* Neutrophils and snail orchestrate the establishment of a pro-tumor microenvironment in lung cancer. *Cell Report* **21**, 3190–3204 (2017).
- [37] Li, C.-Y. *et al.* Initial stages of tumor cell-induced angiogenesis: evaluation via skin window chambers in rodent models. *J. Nat. Cancer Institute* **92**, 143–147 (2000). URL <https://doi.org/10.1093/jnci/92.2.143>. <https://academic.oup.com/jnci/article-pdf/92/2/143/9996237/143.pdf>.
- [38] Goudon, T. *Mathematics for Modeling and Scientific Computing*. Mathematics and Statistics (Wiley-ISTE, 2016).
- [39] Chatelin, F. Convergence of approximation methods to compute eigenelements of linear operations. *SIAM J. Numer. Anal.* **10**, 939–948 (1973).
- [40] Chatelin, F. The spectral approximation of linear operators with applications to the computation of eigenelements of differential and integral operators. *SIAM Rev.* **23**, 495–522 (1981).
- [41] Erdi, Y. E. Limits of tumor detectability in nuclear medicine and PET. *Molecular imaging and radionuclide therapy* **21**, 23–28 (2012).
- [42] Harenberg, D., Marelli, S., Sudret, B. & Winschel, V. Uncertainty quantification and global sensitivity analysis for economic models. *Quantitative Economics* **10**, 1–41 (2019).
- [43] Saltelli, A. Sensitivity analysis of model output. An investigation of new techniques. *Computational Statistics and Data Analysis* **15**, 211–238 (1993).
- [44] Sobol’, I. Sensitivity estimates for nonlinear mathematical models. *Math. Modell. Comput.* **1**, 407–414 (1993).
- [45] Crestaux, T., Le Maître, O. & Martinez, J.-M. Polynomial chaos expansion for sensitivity analysis. *Reliability Engineering and System Safety* **94**, 1161–1172 (2009).
- [46] Sudret, B. Global sensitivity analysis using polynomial chaos expansions. *Reliability Engineering and System Safety* **93**, 964–979 (2008).
- [47] Ernst, O. G., Mugler, A., Starkloff, H. J. & Ullmann, E. On the convergence of generalized polynomial chaos expansions. *ESAIM: Mathematical Modelling and Numerical Analysis* **46**, 317–339 (2012).
- [48] Le Gratiet, L., Marelli, S. & Sudret, B. Metamodel-based sensitivity analysis: Polynomial chaos expansions and gaussian processes. In Ghanem, R., Higdon, D. & Owhadi, H. (eds.) *Handbook of Uncertainty Quantification*, 1289–1325 (Springer International Publishing, Cham, 2017). URL https://doi.org/10.1007/978-3-319-12385-1_38.
- [49] Saltelli, A. Making best use of model evaluations to compute sensitivity indices. *Computer Physics Comm.* **145**, 280 – 297 (2002). URL <http://www.sciencedirect.com/science/article/pii/S0010465502002801>.
- [50] Bailly, C., Thuru, X. & Quesnel, B. Combined cytotoxic chemotherapy and immunotherapy of cancer: modern times. *NAR Cancer* **2**, 1–20 (2020).
- [51] Galon, J. & Bruni, D. Approaches to treat immune hot, altered and cold tumours with combination immunotherapies. *Nature Rev. Drug Discovery* **18**, 197–218 (2019).
- [52] Galon, J. *et al.* Type, density, and location of immune cells within human colorectal tumors predict clinical outcome. *Science* **313**, 1960–1964 (2006).
- [53] Sharma, P. & Allison, J. The future of immune checkpoint therapy. *Science* **348**, 56–61 (2015).
- [54] Champiat, S. *et al.* Intratumoral immunotherapy: from trial design to clinical practice. *Clin. Cancer Res.* (2020).
- [55] Shekarian, T., Valsesia-Wittmann, S., Caux, C. & Marabelle, A. Paradigm shift in oncology: targeting the immune system rather than cancer cells. *Mutagenesis* **30**, 205–211 (2015).
- [56] Weise, K., Poßner, L., Müller, E., Gast, R. & Knösche, T. R. Pygpc: A sensitivity and uncertainty analysis toolbox for Python. *SoftwareX* **11**, 100450 (2020). URL <https://doi.org/10.1016/j.softx.2020.100450>.
- [57] Herman, J. & Usher, W. SALib: An open-source Python library for sensitivity analysis. *The Journal of Open Source Software* **2**, joss00097 (2017). URL <https://doi.org/10.21105/joss.00097>.
- [58] Perthame, B. *Transport equations in biology*. Frontiers in Math. (Birkhauser, 2007).
- [59] Krein, M. & Rutman, M. Linear operator leaving invariant a cone in a Banach space. *Amer. Math. Soc. Translation* **10**, 199–325 (1962).
- [60] Serre, D. *Matrices: theory and applications*, vol. 216 of *Graduate Texts in Math.* (Springer, 2002).
- [61] Homma, T. & Saltelli, A. Importance measures in global sensitivity analysis of nonlinear models. *Reliability Engineering & System Safety* **52**, 1 – 17 (1996). URL <http://www.sciencedirect.com/science/article/pii/0951832096000026>.

Supplementary material

Cell division operator

The binary division operator (2) is a particular case, and for applications it is relevant to deal with more general expressions. Namely, we have

$$Q(n)(t, z) = -a(z)n(t, z) + \int_z^\infty a(z')k(z|z')n(t, z') dz'. \quad (15)$$

In (15), $a(z')$ is the frequency of division of cells having size z' , and $k(z|z')$ gives the size-distribution that results from the division of a tumor cell with size z' . What is crucial for modeling purposes is the requirement

$$\int_0^z z'k(z'|z) dz' = z,$$

which is related to the principle that cell-division does not change the total mass

$$\int_0^\infty zQ(n) dz = 0.$$

We refer the reader to [15] for examples of such cell-division operators.

Equilibrium states

The equilibrium state is characterized by means of an eigenproblem: we look for $\lambda > 0$ and a non negative function $z \geq 0 \mapsto N(z)$ satisfying (10). The analysis of the existence-uniqueness of the eigenpair (λ, N) can be found in [29], the textbook [58, Theorem 4.6], and, for extension to cases with non constant growth rate V , in [15].

Coming back to the coupled model, we infer that the equilibrium phase corresponds to the situation where the death rate precisely counterbalances the natural exponential growth of the tumor cell population. Let Φ be the solution of

$$-\Delta_x \Phi = \sigma - \frac{1}{|\Omega|} \int_\Omega \sigma(y) dy,$$

endowed with the homogeneous Neumann boundary condition. Note that this quantity is a priori defined; it does not depend on the coupling between tumor cells and immune cells. In a computational perspective, it can thus be pre-computed once for all. The equilibrium mass μ_1 is implicitly defined by the fact that the solution of the stationary equation (11) satisfies the constraint (12). This implicit definition is clarified by the following statement, see [8].

Theorem .1 *Let $g : [0, \infty) \rightarrow [0, \infty]$ be a non decreasing function such that $g(0) = 0$, and let $x \mapsto pS(x) \in L^2(\Omega)$ be a non negative function. If $\ell > 0$ is small enough, there exists a unique $\bar{\mu}_1(\ell) > 0$ such that $C_{\bar{\mu}_1(\ell)}$, solution of the stationary equation (11) satisfies $\int_\Omega \delta C dx = \ell$.*

Theorem .1 requires a smallness assumption; for (2) with a constant division rate a , this is a smallness assumption on a . Numerical experiments have shown different large time behaviors for the evolution problem (1a)-(1e):

- when the source term S is space-homogeneous, the expected behavior seems to be very robust. The immune cell concentration tends to fulfill the constraint (12) as time becomes large, and the size repartition of tumor cells tends to the eigenfunction N . The total mass μ_1 tends to a constant; however the asymptotic value cannot be predicted easily. We again refer the reader to Fig. 2 for an illustration of these facts.
- When S has spacial variations, the asymptotic behavior seems to be much more sensitive to the smallness condition. On short time scale of simulations, we observe alternance of growth and remission phases, and the damping to the equilibrium could be very slow.

These observations bring out the complementary roles of different type of cytotoxic cells [36]. The NK cells could be seen as a space-homogeneous source of immune cells, immediately available to fight against the tumor, at the early stage of tumor growth. In contrast, T -cells need an efficient priming which occurs in the draining lymph nodes, and their sources is therefore non-homogeneously distributed. Eventually, NK and $CD8^+$ T -cells cooperate to the anti-tumor immune response.

Computation of the eigen-elements of the growth-fragmentation equation

It is important to bear in mind the main arguments of the proof of the existence-uniqueness of the eigenpair (λ, N) for the growth-fragmentation equation. Namely, for Λ large enough we consider the *shifted* operator

$$\mathcal{T}_\Lambda N = \Lambda N + \partial_z(VN) + aN - \int_z^\infty a(z')k(z|z')N(z') dz'.$$

Then, we check that the operator \mathcal{T}_Λ which associates to a function f the solution n of $\mathcal{T}_\Lambda n = f$ fulfills the requirements of the Krein-Rutman theorem (roughly speaking, positivity and compactness), see [59]. Accordingly, the quantity of interest λ is related to the leading eigenvalue of \mathcal{T}_Λ . In fact, this reasoning should be applied to a somehow truncated and regularized version of the operator, and the conclusion needs further compactness arguments; nevertheless this is the essence of the proof. In terms of numerical method, this suggests to appeal to the inverse power algorithm, applied to a discretized version of the equation. However, we need to define appropriately the shift parameter Λ . As far as the continuous problem is considered, Λ can be estimated by the parameters of the model [15], but it is critical for practical issues to check whether or not this condition is impacted by the discretization procedure. This information will be used to apply the

inverse power method to the discretized and shifted version of the problem.

Analysis of the discrete problem

The computational domain for the size variable is the interval $[0, R]$ where R is chosen large enough: due to the division processes, we expect that the support of the solution remains essentially on a bounded interval, and the cut-off should not perturb too much the solution. In what follows, the size step $h = z_{i+1} - z_i$ is assumed to be constant. The discrete unknowns N_i , with $i \in \{1, \dots, I\}$ and $h = R/I$, are intended to approximate $N(z_i)$ where $z_i = ih$. The integral that defines the gain term of the division operator is approximated by a simple quadrature rule. For the operator (2) the kernel involves Dirac masses which can be approached by peaked Gaussian. We introduce the operator $\mathcal{T}_\Lambda^h : \mathbb{R}^I \rightarrow \mathbb{R}^I$ defined by

$$\begin{cases} (\mathcal{T}_\Lambda^h N)_i = F_i - F_{i-1} + h(\Lambda + a_i)N_i \\ \quad - h^2 \sum_{j=i}^I a(z_j)k(z_i|z_j)N_j, \\ N_1 = 0 \end{cases} \quad (16)$$

where $F_i = V_{i+1/2}N_i$ represents the convective numerical flux on the grid point $z_{i+1/2} = (i+1/2)h$, $i \in \{1, \dots, I\}$. This definition takes into account that the growth rate is non negative, and applies the upwinding principles. Note that the step size h should be small enough to capture the division of small cells, if any. The following statement provides the a priori estimate which allows us to determine the shift for the discrete problem.

Theorem .2 *We suppose that*

- i) $z \mapsto V(z)$ is a continuous function which lies in L^∞ and it is bounded from below by a positive constant,
- ii) $h \sum_{j=1}^I a(z_j)k(z_i|z_j)$ remains bounded uniformly with respect to h ,
- iii) for any $i \in \{1, \dots, I-1\}$, there exists $j \in \{i+1, \dots, I\}$ such that $a(z_j)k(z_i|z_j) > 0$,
- iv) there exists $Z_0 \in (0, \infty)$ such that, setting $\bar{N}(z) = h \sum_{j=2}^I k(z_j|z)$, we have $a(z)(\bar{N}(z) - 1) \geq \nu_0 > 0$ for any $z \geq Z_0$.

Let

$$\Lambda > \frac{\|V\|_{L^\infty}}{\min_{j \in \{1, \dots, I\}} |V_{j+1/2}|} \max_{k \in \{1, \dots, I\}} \left(h \sum_{j=k}^I a_j k(z_k|z_j) \right) - \min_{j \in \{1, \dots, I\}} |a_j|, \quad (17)$$

and we suppose that $R > Z_0$ is large enough. Then, \mathcal{T}_Λ^h is invertible and there exists a pair $\mu > 0$, $N \in \mathbb{R}^I$ with positive components, such that $\text{Ker}((\mathcal{T}_\Lambda^h)^{-1} - \mu) = \text{Span}\{N\}$. Moreover $\lambda = \Lambda - \frac{1}{\mu} > 0$.

Note that the sum that defines $\bar{N}(z)$ is actually reduced over the indices such that $jh \leq z$; this quantity is interpreted as the expected number of cells produced from the division of a cell with size z so that the forth assumption is quite natural.

Proof. Let $f \in \mathbb{R}^I$. We consider the equation

$$\mathcal{T}_\Lambda^h N = f.$$

We denote $N = \mathcal{S}_\Lambda^h f$ the solution. We are going to show that \mathcal{S}_Λ^h is well defined and satisfies the assumptions of the Perron-Frobenius theorem, see e. g. [38, Theorem 1.37 & Corollary 1.39] or [60, Chapter 5].

It is convenient to introduce the change of unknown $U_i = N_i V_{i+1/2}$, $\forall i \in \{1, \dots, I\}$. The problem recasts as

$$\begin{cases} (\widetilde{\mathcal{T}}_\Lambda^h U)_i = h \frac{f_i}{V_{i+1/2}}, \text{ with} \\ (\widetilde{\mathcal{T}}_\Lambda^h U)_i = U_i - U_{i-1} + h \frac{\Lambda + a_i}{V_{i+1/2}} U_i \\ \quad - h^2 \sum_{j=i}^I \frac{a_j}{V_{j+1/2}} k(z_i|z_j) U_j, \\ U_1 = 0. \end{cases} \quad (18)$$

The solution is interpreted as the fixed point of the mapping

$$\xi \longmapsto U = A^h \xi$$

where U is given by $U_1 = 0$ and

$$U_i = U_{i-1} + h^2 \sum_{j=i}^I \frac{a_j}{V_{j+1/2}} k(z_i|z_j) \xi_j + h \frac{f_i}{V_{i+1/2}}.$$

We are going to show that A^h is a contraction: $\|A^h \xi\|_{\ell^\infty} \leq k \|\xi\|_{\ell^\infty}$ for some $k < 1$. Multiplying (18) by $\text{sign}(U_i)$, we obtain

$$\begin{aligned} \left(1 + h \frac{\Lambda + a_i}{V_i}\right) \text{sign}(U_i) U_i &= \left(1 + h \frac{\Lambda + a_i}{V_i}\right) |U_i| \\ &= \text{sign}(U_i) U_{i-1} + h^2 \sum_{j=i}^I \frac{a_j}{V_{j+1/2}} k(z_i|z_j) \text{sign}(U_i) \xi_j \\ &\leq |U_{i-1}| + h^2 \sum_{j=i}^I \frac{a_j}{V_{j+1/2}} k(z_i|z_j) |\xi_j|. \end{aligned}$$

We multiply this by the weight $\prod_{l=1}^{i-1} [1 + h \frac{\Lambda + a_l}{V_{l+1/2}}]$, where all factors are ≥ 1 . We get

$$\begin{aligned} |U_i| \prod_{l=1}^i \left[1 + h \frac{\Lambda + a_l}{V_{l+1/2}}\right] &\leq |U_{i-1}| \prod_{l=1}^{i-1} \left[1 + h \frac{\Lambda + a_l}{V_{l+1/2}}\right] \\ &\quad + h^2 \prod_{l=1}^i \left[1 + h \frac{\Lambda + a_l}{V_{l+1/2}}\right] \sum_{j=i}^I \frac{a_j}{V_{j+1/2}} k(z_i|z_j) |\xi_j|. \end{aligned}$$

Then, summing over $i \in \{2, \dots, m\}$ yields

$$\begin{aligned} |U_m| & \prod_{l=1}^m \left[1 + h \frac{\Lambda + a_l}{V_{l+1/2}} \right] \\ & \leq |U_1| \left[1 + h \frac{\Lambda + a_1}{V_{3/2}} \right] \\ & \quad + h^2 \sum_{i=2}^m \prod_{l=1}^i \left[1 + h \frac{\Lambda + a_l}{V_{l+1/2}} \right] \sum_{j=i}^I \frac{a_j}{V_{j+1/2}} k(z_i|z_j) |\xi_j| \end{aligned}$$

where actually $U_1 = 0$. It follows that

$$\begin{aligned} |U_m| & \leq h^2 \sum_{i=2}^m \prod_{l=1}^i \left[1 + h \frac{\Lambda + a_l}{V_{l+1/2}} \right]^{-1} \sum_{j=i}^I \frac{a_j}{V_{j+1/2}} k(z_i|z_j) |\xi_j| \\ & \leq \frac{h^2 \|\xi\|_{\ell^\infty}}{\min_{j \in \{1, \dots, I\}} V_{j+1/2}} \sum_{i=2}^m \prod_{l=1}^i \left[1 + h \frac{\Lambda + a_l}{V_{l+1/2}} \right]^{-1} \sum_{j=i}^I a_j k(z_i|z_j) \\ & \leq \frac{h^2 \|\xi\|_{\ell^\infty}}{\min_{j \in \{1, \dots, I\}} V_{j+1/2}} \left\| \sum_{j=i}^I a_j k(z_i|z_j) \right\|_{\ell^\infty} \\ & \quad \sum_{i=2}^m \left[1 + h \frac{\Lambda + \min_{l \in \{1, \dots, I\}} a_l}{\|V\|_{L^\infty}} \right]^{i-m+1} \\ & \leq \frac{h \|\xi\|_{\ell^\infty}}{\min_{j \in \{1, \dots, I\}} V_{j+1/2}} \left\| \sum_{j=i}^I a_j k(z_i|z_j) \right\|_{\ell^\infty}^{-1} \\ & \quad \left[\frac{\Lambda + \min_{l \in \{1, \dots, I\}} a_l}{\|V\|_{L^\infty}} \right]^{-1}. \end{aligned}$$

Therefore, A^h is a contraction provided (17) holds. This estimate is similar to the condition obtained for the continuous problem, see [15, Proof of Theorem 2, Appendix B]; the discretization does not introduce further constraints.

We are now going to show that \mathcal{T}_Λ^h is a M -matrix when (17) holds. Let $f \in \mathbb{R}^I \setminus \{0\}$ with non negative components. Let $U \in \mathbb{R}^I$ satisfy $(\mathcal{T}_\Lambda^h U)_i = h \frac{f_i}{V_{i+1/2}}$. Let i_0 be the index such that $U_{i_0} = \min \{U_i, i \in \{2, \dots, I\}\}$. We have

$$\begin{aligned} U_{i_0} & \left(1 + h \frac{\Lambda + a_{i_0}}{V_{i_0+1/2}} \right) \\ & = U_{i_0-1} + h^2 \sum_{j=i_0}^I \frac{a_j}{V_{j+1/2}} k(z_{i_0}|z_j) U_j + h \frac{f_{i_0}}{V_{i_0+1/2}} \\ & \geq U_{i_0} \left(1 + h^2 \sum_{j=i_0}^I \frac{a_j}{V_{j+1/2}} k(z_{i_0}|z_j) \right) + h \frac{f_{i_0}}{V_{i_0+1/2}}. \end{aligned} \quad (19)$$

Since $f_{i_0} \geq 0$, we get

$$U_{i_0} \underbrace{\left(\frac{\Lambda + a_{i_0}}{V_{i_0+1/2}} - h \sum_{j=i_0}^I \frac{a_j}{V_{j+1/2}} k(z_{i_0}|z_j) \right)}_{>0 \text{ by (17)}} \geq 0,$$

which tells us that $U_{i_0} \geq 0$. Suppose $U_{i_0} = 0$ for some $i_0 > 1$. Coming back to (19), we deduce that U_{i_0-1} vanishes too, and so on and so forth, we obtain $U_1 = \dots = U_{i_0} = 0$. Finally, we use the irreducibility assumption iii): we can find $j_0 > i_0$ such that $\frac{a_{j_0}}{V_{j_0+1/2}} k(z_{i_0}|z_{j_0}) > 0$ and (19) implies $\frac{a_{j_0}}{V_{j_0+1/2}} k(z_{i_0}|z_{j_0}) U_{j_0} = 0$, so that $U_{j_0} = 0$. We deduce that

$U = 0$, which contradicts $f \neq 0$. Therefore the components of U are positive, but U_1 .

We conclude by applying the Perron-Frobenius theorem to $(\mathcal{T}_\Lambda^h)^{-1}$, [60, Chapter 5]. It remains to prove that $\lambda = \Lambda - \frac{1}{\mu}$ is positive, with μ the spectral radius of $(\mathcal{T}_\Lambda^h)^{-1}$. To this end, we make use of assumption iv). We set $Z_0 = i_0 h$. We argue by contradiction, supposing that $\lambda = \Lambda - 1/\mu < 0$. We consider the eigenvector with positive components and normalized by the condition $h \sum_{i=1}^I U_i = 1$. We have

$$\begin{aligned} (\widetilde{\mathcal{T}}_0^h U)_i & = U_i - U_{i-1} + \frac{a_i}{V_{i+1/2}} h U_i \\ & \quad - h^2 \sum_{j=i}^I \frac{a_j}{V_{j+1/2}} k(z_i|z_j) U_j = -\lambda U_i \geq 0. \end{aligned}$$

It follows that, for $m \geq i_0$,

$$\begin{aligned} U_m & \geq -h \sum_{i=2}^m \frac{a_i}{V_{i+1/2}} U_i + h^2 \sum_{i=2}^m \sum_{j=i}^I \frac{a_j}{V_{j+1/2}} k(z_i|z_j) U_j \\ & \geq -h \sum_{i=2}^m \frac{a_i}{V_{i+1/2}} U_i + h \sum_{j=2}^m \left(h \sum_{i=2}^j k(z_i|z_j) \right) \frac{a_j}{V_{j+1/2}} U_j \\ & \geq -h \sum_{i=2}^m \frac{a_i}{V_{i+1/2}} U_i + h \sum_{j=2}^m \bar{\mathcal{N}}(z_j) \frac{a_j}{V_{j+1/2}} U_j \\ & \geq h \sum_{i=2}^m (\bar{\mathcal{N}}(z_i) - 1) \frac{a_i}{V_{i+1/2}} U_i \\ & \geq h \sum_{i=i_0}^m (\bar{\mathcal{N}}(z_i) - 1) \frac{a_i}{V_{i+1/2}} U_i \geq \frac{\nu_0}{\|V\|_{L^\infty}} h \sum_{i=i_0}^m U_i. \end{aligned}$$

It implies

$$1 = h \sum_{m=1}^I U_m \geq h \sum_{m=i_0}^I U_m \geq h(I - i_0) \frac{\nu_0}{\|V\|_{L^\infty}} h \sum_{i=i_0}^m U_i.$$

We arrive at

$$1 \geq (R - Z_0) \frac{\nu_0}{\|V\|_{L^\infty}},$$

a contradiction when R is chosen large enough (but how large R should be does not depend on h). Therefore, we conclude that $\lambda > 0$. ■

Numerical approximation of (λ, N)

We compute (an approximation of) the eigenpair (λ, N) by using the inverse power method which finds the eigenvalue of $(\mathcal{T}_\Lambda^h)^{-1}$ with largest modulus:

- We pick Λ verifying (17).
- We compute once for all the LU decomposition of the matrix \mathcal{T}_Λ^h .
- We choose a threshold $0 < \epsilon \ll 1$.
- We start from a random vector $N^{(0)}$ and we construct the iterations

$$-LUq^{(k+1)} = N^{(k)},$$

$$-N^{(k+1)} = \frac{q^{(k+1)}}{\|q^{(k+1)}\|}$$

until the relative error $\frac{\|N^{(k+1)} - N^{(k)}\|}{\|N^{(k)}\|} \leq \epsilon$ is small enough.

Then, given the last iterate $N^{(K)}$, we set $LUq = N^{(K)}$, $\tilde{\mu} = \frac{q \cdot N^{(K)}}{N^{(K)} \cdot N^{(K)}}$, and $\tilde{\lambda} = \Lambda - 1/\tilde{\mu}$.

This approach relies on the ability to approximate correctly the eigenpair of the growth-fragmentation operator. In particular, it is important to preserve the algebraic multiplicity. This issue is quite subtle and it is known that the pointwise convergence of the operator is not enough to guarantee the convergence of the eigenelements and the consistency of the invariant subspaces, see [39] for relevant examples. This question has been thoroughly investigated in [39, 40] which introduced a suitable notion of stability. It turns out that one needs a uniform convergence of the operators. Namely, here, we should check that $\|(\mathcal{T}_\Lambda^I)^{-1} - (\mathcal{T}_\Lambda)^{-1}\| \rightarrow 0$ as $I \rightarrow \infty$. In the present framework, a difficulty relies on the fact that the size variable lies in an unbounded domain, which prevents for using usual compactness arguments. For this reason, we introduce a truncated version of the problem, which has also to be suitably regularized. Let us denote by $\mathcal{T}_\Lambda^{R,\epsilon}$ the corresponding operator, where ϵ represents the regularization parameter. This truncated and regularized operator appeared already in [15]. Indeed, we know from [15] that $\|\mathcal{T}_\Lambda^{R,\epsilon} - \mathcal{T}_\Lambda\| \rightarrow 0$ as $R \rightarrow \infty$ and $\epsilon \rightarrow 0$, hence, this implies that $\|(\mathcal{T}_\Lambda^{R,\epsilon})^{-1} - (\mathcal{T}_\Lambda)^{-1}\| \rightarrow 0$ as $R \rightarrow \infty$ and $\epsilon \rightarrow 0$ by continuity of the map $\Pi : \mathcal{T}_\Lambda \mapsto (\mathcal{T}_\Lambda)^{-1}$. Moreover, $(\mathcal{T}_\Lambda^{R,\epsilon})^{-1}$ is well-defined, continuous and compact, see [15, Appendix. B]. The discrete operators $(\mathcal{T}_\Lambda^I)^{-1}$ converge pointwise to $(\mathcal{T}_\Lambda^{R,\epsilon})^{-1}$, and the compactness of $(\mathcal{T}_\Lambda^{R,\epsilon})^{-1}$ ensures that the discrete operator converges uniformly to $(\mathcal{T}_\Lambda^{R,\epsilon})^{-1}$, for $0 < R < \epsilon$ and $0 < \epsilon < 1$ fixed (see [40] for more details on this fact). Following [40], we deduce that the numerical eigenelements (λ^I, N^I) converges to $(\lambda^{R,\epsilon}, N^{R,\epsilon})$, the eigenelements of $(\mathcal{T}_\Lambda^{R,\epsilon})^{-1}$, while preserving their algebraic multiplicity. Finally the uniform convergence $\|(\mathcal{T}_\Lambda^{R,\epsilon})^{-1} - (\mathcal{T}_\Lambda)^{-1}\| \rightarrow 0$ as $R \rightarrow \infty$ and $\epsilon \rightarrow 0$ ensures the convergence of $(\lambda^{R,\epsilon}, N^{R,\epsilon})$ to (λ, N) , [15].

Numerical results

For some specific fragmentation kernels and growth rates, the eigenpair (λ, N) is explicitly known, see [15]. We can use these formula to check that the algorithm is able to find the expected values and profiles. To this end, we introduce the relative errors

$$E_\lambda^h = \frac{|\lambda - \tilde{\lambda}|}{\tilde{\lambda}} \quad \text{and} \quad E_V^h = h \sum_{i=1}^I |N_i^{(K)} - N(ih)|$$

where $N^{(K)}$ and N are both normalized by $h \sum_{i=1}^I N_i^{(K)} = h \sum_{i=1}^I N(ih) = 1$.

Mitosis fragmentation kernel. We start with the binary division kernel:

$$k(z|z') = \delta_{z'=2z}. \quad (20)$$

The associated division operator is described by (2). We assume that a and V are constant. In this specific case the eigenpair is given by

$$\lambda = a, \quad N(z) = \bar{N} \sum_{n=0}^{\infty} (-1)^n \alpha_n \exp\left(-2^{n+1} \frac{a}{V} z\right), \quad (21)$$

with $\bar{N} > 0$ an appropriate normalizing constant and $(\alpha_n)_{n \in \mathbb{N}}$ is the sequence defined by the recursion

$$\alpha_0 = 1, \quad \alpha_n = \frac{2}{2^n - 1} \alpha_{n-1}.$$

In practice we shall use a truncated version of the series that defines N . For the numerical tests, we use the parameters collected in Table 3

a	V	R	ϵ
4	0.6	5	10^{-6}

Table 3. Data for the numerical tests: binary division kernel

Number of cells	E_λ	E_V
1000	3.73×10^{-5}	3.83×10^{-2}
2000	5.68×10^{-8}	1.93×10^{-2}
4000	6.77×10^{-7}	9.69×10^{-3}
8000	6.84×10^{-7}	4.85×10^{-3}

Table 4. Binary division kernel: errors for several number of grid points

With this threshold ϵ , the approached eigenpair is reached in 43 iterations, independently of the size step. Fig. 7 represents the evolution of the error E_V^h as a function of h in a log-log scale: $N^{(K)}$ approaches N at order 1. The rate improves when using a quadrature rule with a better accuracy. For this test, the approximation of the eigenvalue is already accurate with a coarse grid; it is simply driven by the threshold ϵ and E_L^h does not significantly change with h .

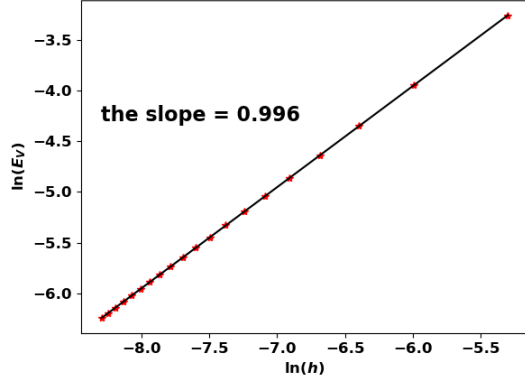
Uniform fragmentation. The uniform fragmentation kernel is defined by:

$$k(z|z') = \frac{1}{z'} \mathbb{1}_{0 \leq z \leq z'}.$$

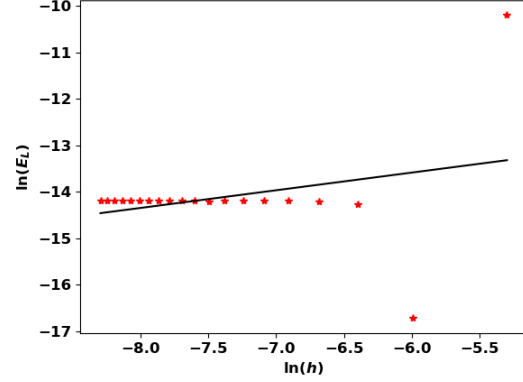
We apply the algorithm for the following two cases:

1. $V(z) = V_0$ and $a(z) = a_0 z$. We have $\lambda = \sqrt{a_0 V_0}$ and

$$N(z) = 2\sqrt{\frac{a_0}{V_0}} \left(Z + \frac{Z^2}{2} \right) \exp\left(-Z - \frac{Z^2}{2}\right).$$



(a) The rate of convergence to the exact eigenfunction with respect to h



(b) The rate of convergence to the exact eigenvalue with respect to h

Figure 7. Binary division kernel: convergence rates of $(\lambda^{(K)}, N^{(K)})$ with respect to h

We still use the values in Table 3 (especially, $a_0 = a$ and $V_0 = V$). The approximated eigenpair is obtained in 84 iterations and, as in the previous test, it does not change with the size step. In this case, both the eigenvalue and the eigenfunction are approached at order 1, see Table 5 and Fig. 8.

1187

$n = 1$	$\lambda = V_0$	$N(z) = \frac{a_0}{V_0} \exp\left(-\frac{a_0}{V_0} z\right)$
$n = 2$	$\lambda = V_0$	$N(z) = \frac{2a_0}{\pi V_0} \exp\left(-\frac{a_0}{2V_0} z^2\right)$
n	$\lambda = V_0$	$N(z) = \left(\frac{a_0}{nV_0}\right)^{\frac{1}{n}} \frac{n}{\Gamma(\frac{1}{n})} \exp\left(-\frac{a_0}{nV_0} z^n\right)$

Number of cells	E_λ	E_V
1000	1.30×10^{-2}	8.89×10^{-3}
2000	6.43×10^{-3}	4.50×10^{-3}
4000	3.23×10^{-3}	2.24×10^{-3}
8000	1.62×10^{-3}	1.13×10^{-3}

Table 5. Uniform fragmentation, ex. 1: errors for several number of grid points

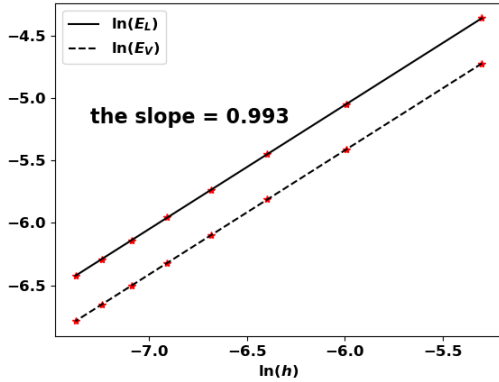


Figure 8. Uniform fragmentation, ex. 1: rate of convergence to the exact eigenpair with respect to h

Note that the growth rate V vanishes and Theorem .2 does not apply as such. Nonetheless, the algorithm works well and still captures the eigenpair. We perform the test for $n = 1$ and $n = 2$ and the results are recorded in Table 6, Fig. 9 and Table 7, Fig. 10, respectively.

Number of cells	E_λ	E_V
1000	4.70×10^{-2}	2×10^{-2}
2000	2.43×10^{-2}	1.06×10^{-2}
4000	1.25×10^{-2}	5.5×10^{-3}
8000	6.39×10^{-3}	2.81×10^{-3}

Table 6. Uniform fragmentation, ex. 2, case $n = 1$: errors for different number of cells

2. $V(z) = V_0 z$ and $a(z) = a_0 z^n$ with $n \in \mathbb{N} \setminus \{0\}$. The eigenpair is defined by the following formula:

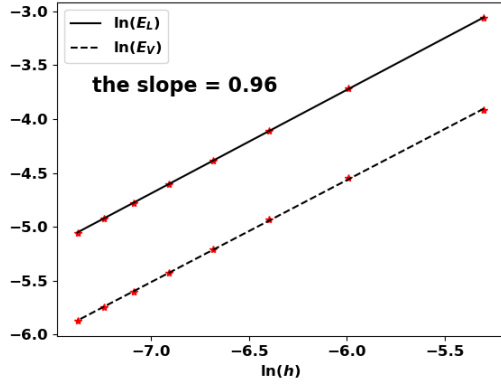


Figure 9. Uniform fragmentation, ex. 2 case $n = 1$: rate of convergence to the exact eigenpair with respect to h

Number of cells	E_λ	E_V
1000	2.39×10^{-2}	8.81×10^{-2}
2000	1.23×10^{-3}	4.53×10^{-3}
4000	6.41×10^{-3}	2.35×10^{-3}
8000	3.41×10^{-3}	1.24×10^{-3}

Table 7. Uniform fragmentation, ex. 2, case $n = 2$: errors for different number of cells

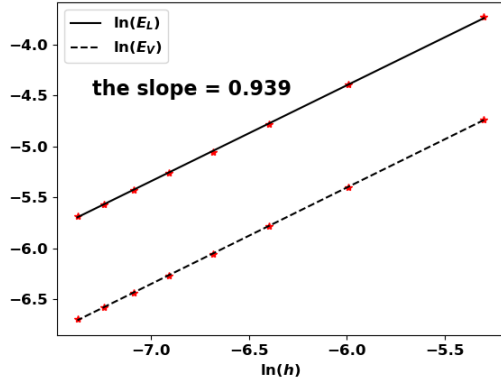


Figure 10. Uniform fragmentation, ex. 2: rate of convergence to the exact eigenpair with respect to h

Sensitivity analysis on the equilibrium mass

Having an efficient procedure to predict the residual mass of the equilibrium phase also opens perspectives to discuss the influence of the parameters. This can provide useful hints for the design and the optimization of anti-tumor therapies. We address this issue by performing a global sensitivity analysis on the immune-controlled tumor mass. Sensitivity analysis

also provides information on the quantification of uncertainty in the model output with respect to the uncertainties in the input parameters. We remind the reader that the equilibrium mass is seen as a function of the parameters in Table 1:

$$\mu_1 = f(a, A, p, \chi, D, \gamma). \quad (22)$$

We consider that the input parameters are independent random variables uniformly distributed in an interval $[x_1, x_2] \subset (0, \infty)$:

$$M = (a, A, p, \chi, D, \gamma) \text{ with } M_i \sim U(x_1, x_2). \quad (23)$$

The pillar of the Sobol sensitivity analysis is the decomposition of f into $2^n - 1$ summands of increasing dimensions:

$$f(M) = f_0 + \sum_{i=1}^n f_i(M_i) + \sum_{1 \leq i < j \leq n} f_{ij}(M_i, M_j) + \dots + f_{1\dots n}(M_1, \dots, M_n), \quad (24)$$

where

$$\frac{1}{x_2 - x_1} \int_{[x_1, x_2]} f_{i_1 \dots i_p}(M_{i_1 \dots i_p}) dM_{i_k} = 0 \quad \text{for } k \in \{1, \dots, p\}, \quad (25)$$

$$f_0 = \frac{1}{(x_2 - x_1)^n} \int_{[x_1, x_2]^n} f(M) dM, \quad (26)$$

$$\int_{[x_1, x_2]^n} f_{i_1 \dots i_p}(M_{i_1 \dots i_p}) f_{j_1 \dots j_p}(M_{j_1 \dots j_p}) dM = 0, \quad (27)$$

and $M_{i_1 \dots i_p} = (M_{i_1}, \dots, M_{i_p})$. The existence and uniqueness of the above decomposition has been proven in [44], given f a square integrable function. Owing to the orthogonality condition (27), the total variance of f reads:

$$\mathcal{V} = \text{Var}(f(M)) = \frac{1}{(x_2 - x_1)^n} \int_{[x_1, x_2]^n} f(M)^2 dM - f_0^2. \quad (28)$$

Given (24), \mathcal{V} can be decomposed as follows:

$$\mathcal{V} = \sum_{i=1}^n \mathcal{V}_i + \sum_{1 \leq i < j \leq n} \mathcal{V}_{ij} + \dots + \mathcal{V}_{1\dots n}, \quad (29)$$

where the terms $\mathcal{V}_{i_1 \dots i_p}$, called partial variances read:

$$\mathcal{V}_{i_1 \dots i_p} = \frac{1}{(x_2 - x_1)^n} \int_{[x_1, x_2]^n} f_{i_1 \dots i_p}^2 dM_{i_1} \dots dM_{i_p}. \quad (30)$$

Following the description in [44], the Sobol' sensitivity indices are defined as follows:

$$S_{i_1 \dots i_p} = \frac{\mathcal{V}_{i_1 \dots i_p}}{\mathcal{V}}. \quad (31)$$

They verify

$$\sum_{i=1}^n S_i + \sum_{1 \leq i < j \leq n} S_{ij} + \dots + S_{1\dots n} = 1. \quad (32)$$

Each index $S_{i_1 \dots i_p}$ measures how the total variance of f is affected by uncertainties in the set of input parameters $i_1 \dots i_p$. An equivalent definition of the above indices is given by (see [43]):

$$\mathcal{V}_i = \text{Var}(\mathbb{E}(Y|M_i)), \quad \mathcal{V}_{ij} = \text{Var}(\mathbb{E}(Y|M_i, M_j)) - \mathcal{V}_i - \mathcal{V}_j, \dots \quad (33)$$

The total effect of a specific input parameter i is evaluated by the so-called total sensitivity index $S_T^{(i)}$, the sum of the sensitivity indices which contain i :

$$S_T^{(i)} = \sum_{C_i} S_{i_1 \dots i_p} \quad (34)$$

where $C_i = \{(i_1 \dots i_p) : \exists m \in \{1, \dots, p\}, i_m = i\}$. In practice, the sensitivity indices that are needed to discriminate the impact of the parameters are the first, second and total Sobol' sensitivity indices. The above indices are computed using Monte Carlo simulations combined with a careful sampling of the parameters space in order to reduce the computational load and the number of model evaluations. For this purpose, the following estimators can be derived using two different N samples A and B , see [43, 49],

$$\hat{f}_0 = \frac{1}{N} \sum_{l=1}^N f(M_l), \quad (35)$$

$$\hat{\mathcal{V}} = \frac{1}{N} \sum_{l=1}^N f^2(M_l) - \hat{f}_0^2, \quad (36)$$

$$\hat{\mathcal{V}}_i = \frac{1}{N} \sum_{l=1}^N f(M_{(-i)l}^{(A)}, M_{il}^{(A)}) f(M_{(-i)l}^{(B)}, M_{il}^{(A)}) - \hat{f}_0^2, \quad (37)$$

$$\begin{aligned} \hat{\mathcal{V}}_{ij} &= \frac{1}{N} \sum_{l=1}^N f(M_{-(i,j)l}^{(A)}, M_{il}^{(A)}, M_{jl}^{(A)}) f(M_{-(i,j)l}^{(B)}, M_{il}^{(A)}, M_{jl}^{(A)}) \\ &\quad - \hat{f}_0^2 - \hat{\mathcal{V}}_i - \hat{\mathcal{V}}_j. \end{aligned} \quad (38)$$

Here the notation $M_{-(i_1 \dots i_p)l}$ stands for the l -th sample line where we get rid of the points corresponding to the indices i_1, \dots, i_p . The total sensitivity [61] is given by:

$$S_{T_i} = 1 - S_{-i} \quad (39)$$

where S_{-i} is the sum of all the sensitivity indices that do not contain the index i . Hence, the total sensitivity index estimator reads:

$$\hat{S}_{T_i} = 1 - \frac{\hat{\mathcal{V}}_{-i}}{\hat{\mathcal{V}}} \quad (40)$$

where

$$\hat{\mathcal{V}}_{-i} = \frac{1}{N} \sum_{l=1}^N f(M_{(-i)l}^{(A)}, M_{il}^{(A)}) f(M_{(-i)l}^{(B)}, M_{il}^{(B)}) - \hat{f}_0^2.$$